الجمهورية الجزائرية الديمقراطية الشعبية
République Algérienne Démocratique et Populaire
وزارة التعليم العالي والبحث العلمي
Ministère de l'Enseignement Supérieur et de la Recherche Scientifique
جامعة الشهيد الشيخ العربي التبسي - تبسة

Mémoire

Présenté pour obtenir le diplôme de

Master

Spécialité : Energétique

Filière : Génie mécanique

ETUDE ET ANALYSE D'UNE EOLIENNE A L'AIDE DU LOGICIEL QBLADE

Présenté par :

BOUFAROU Mohamed Akram

Mémoire soutenu le 04 / 06 / 2026 devant le jury composé de

Président :	**Dr. MEKAHLIA Alaeddine**	MCB
Encadreur :	**Dr. LAOUAR Roudouane**	MCA
Examinateur :	**Mr. GHANAIA Saddek**	MAA

Année universitaire :2025/2026

CamScanner

Acknowledgements

I deeply thank Allah Almighty, who has granted me success and bestowed upon me the patience and strength to complete this humble work; for without His divine guidance and grace, this study would not have seen the light.

First and foremost, I would like to express my profound gratitude and appreciation to my role model in science and research, my supervisor, **Dr. Roudouane Laouar**, for his invaluable guidance and continuous support throughout the realization of this interesting and important research. I am deeply thankful for his immense patience in teaching me fundamental concepts, defining the scientific vision, and providing key insights that served as gateways to vast research horizons.

I also extend my sincere thanks and appreciation to my honorable professor, **Mr.Alaaeddine Mekahlia**, for his dedicated efforts, meticulous supervision, and valuable guidance that greatly enriched my academic attainment and helped refine this research.

My gratitude is also extended to all the respected professors of the Department of Mechanical Engineering, and to all the educators who contributed from near or far to building my scientific background and guiding my academic path.

Finally, I would like to thank everyone who extended a helping hand, offered support, or dedicated their valuable time to help me successfully achieve this work. To all of you, I offer my highest respect and deepest gratitude.

DEDICATION

To those who have been a true source of support at every step of this journey...

To my dear parents, who spared neither effort nor sacrifice to help me reach this milestone in my life. I express my deepest gratitude and lifelong recognition to them.

To my beloved brothers and sisters, especially my brother ***Aymen****, who was my primary pillar of support. May Allah reward him generously and grant him His boundless blessings.*

I dedicate this work to ***SIAD Safa****, my companion along the way and the steadfast pillar upon whom I can always rely. When everything else collapses around me, she remains my ultimate refuge and the true source of my happiness.*

I also offer this achievement to the entire ***PEST 2020-2025 promotion****, and more specifically to my classmates in* ***Mechanical Engineering****, my fellow companions on this path.*

I would like to express my profound gratitude to my dear comrades of this academic year: ***Mohamed Zerouali****,* ***Nedjm Eddine Saoud****, and* ***Dhia Bachouat****. Thank you for sharing this journey with me and for being an unwavering support at every single stage.*

I wish you all a brilliant professional career and a life filled with success.

ملخص:

تتناول هذه المذكرة التصميم الأيروديناميكي، النمذجة الرقمية، والتحسين البارامتري لروتور عنفة رياح صغيرة الحجم باستخدام برنامج المحاكاة المتخصص QBlade. تهدف الدراسة بشكل أساسي إلى معالجة الموازنة الدقيقة بين رفع الكفاءة الأيروديناميكية وضمان السلامة الهيكلية للشفرات عند الاشتغال في مستويات منخفضة لعدد رينولدز وظروف جريان مضطربة. اعتمد الإطار النظري للبحث على نظرية كمية الحركة لعنصر الشفرة (BEM) مدعومة بتصحيحات "براندتل" لضياعات الأطراف وتصحيح "غلاويرت" للدفع العالي.

أظهرت نتائج المحاكاة الرقمية أن تبني تشكيلة شفرات هجينة (بدمج المقطع الأيروديناميكي السميك SG6040عند جذر الشفرة والمقطع عالي الكفاءة SG6043عند الأطراف) يمثل استراتيجية هندسية ممتازة لعزل عزوم الانحناء الميكانيكية العالية مع الحفاظ على أقصى استخلاص ممكن للطاقة. كما بينت الدراسة البارامترية أن المتغيرات الهندسيّة (كعدد الشفرات، توزيع الوتر، وزاوية الالتواء) تؤثر بشكل حاسم على أداء العنفة؛ حيث حقق التصميم ذو الثلاث شفرات الموازنة الأيروديناميكية المثلى، في حين أدى الارتفاع المفرط في عدد الشفرات إلى انهيار معامل القدرة (Cp) والاستطاعة الكلية نتيجة هيمنة قوى كبح السحب وظاهرة الحظر الأيروديناميكي وتداخل الدوامات الخلفية. أخيرًا، أكد تحليل الإجهادات الهيكلية (Von Mises) السلامة الميكانيكية للتصميم المقترح وبقاء الإجهادات ضمن الحدود المسموحة للمادة.

Abstract:

This thesis presents the aerodynamic design, numerical modeling, and parametric optimization of a small-scale wind turbine rotor using the specialized simulation software **QBlade**. The primary objective of this study is to address the delicate trade-off between maximizing aerodynamic efficiency and ensuring structural integrity under low Reynolds number operating conditions and turbulent flows. The theoretical framework relies on the Blade Element Momentum (BEM) theory, augmented with Prandtl's tip loss and Glauert's high-thrust corrections.

The numerical simulation results demonstrate that implementing a hybrid blade configuration (deploying the thicker SG6040 airfoil at the blade root and the highly efficient SG6043 airfoil at the tip) serves as an excellent engineering strategy to isolate high mechanical bending moments while maximizing energy extraction. Furthermore, the parametric study reveals that geometric variables (such as blade count, chord distribution, and twist angle) drastically influence performance. The 3-blade layout achieves the optimum aerodynamic balance, whereas an excessive increase in blade count leads to a sharp decline in the power coefficient (Cp) and total power due to parasitic drag dominance, aerodynamic blockage, and wake interaction. Finally, the structural analysis confirms that the Von Mises stress distribution remains safely within the permissible material yield thresholds, validating the viability of the optimized design.

Résumé:

Cette thèse présente la conception aérodynamique, la modélisation numérique et l'optimisation paramétrique d'un rotor d'éolienne de petite puissance à l'aide du logiciel de simulation dédié **QBlade**. L'objectif principal de cette étude est de traiter le compromis délicat entre la maximisation de l'efficacité aérodynamique et la garantie de l'intégrité structurelle sous des conditions de fonctionnement à faible nombre de Reynolds et d'écoulements turbulents. Le cadre théorique repose sur la théorie de la quantité de mouvement de l'élément de pale (BEM), augmentée des corrections de perte en bout de pale de Prandtl et de forte poussée de Glauert.

Les résultats des simulations numériques démontrent que l'implémentation d'une configuration de pale hybride (déployant le profil aérodynamique plus épais SG6040 à la racine de la pale et le profil hautement efficace SG6043 à l'extrémité) constitue une excellente stratégie d'ingénierie pour isoler les moments de flexion mécanique élevés tout en maximisant l'extraction d'énergie. De plus, l'étude paramétrique révèle que les variables géométriques (telles que le nombre de pales, la distribution de la corde et l'angle de vrillage) influencent considérablement les performances. La configuration à 3 pales atteint l'équilibre aérodynamique optimal, tandis qu'une augmentation excessive du nombre de pales entraîne une chute brutale du coefficient de puissance (Cp) et de la puissance totale en raison de la dominance de la traînée parasite, du blocage aérodynamique et de l'interaction des sillages. Enfin, l'analyse structurelle confirme que la distribution des contraintes de Von Mises reste largement en dessous des seuils d'élasticité admissibles du matériau, validant la viabilité de la conception optimise.

TABLE OF CONTENTS

GENERAL INTRODUCTION 1

CHAPTER I 4

I.1 INTRODUCTION 5
I.2 OVERVIEW OF WIND ENERGY 5
I.2.1 DEFINITION OF WIND 5
I.2.2 WIND ENERGY CONCEPT 5
I.3 WIND ENERGY CONVERSION CHAIN 5
I.3.1 KENETIC TO MECHANICAL 5
I.3.2 MECHANICAL TO ELECTRICAL 5
I.4 WIND ENERGY POTENTIAL 6
I.4.1 VERTICAL WIND SPEED GRADIENT 6
I.4.2 WEIBULL DISTRIBUTION 6
I.5 CLASSIFICATION OF WIND FARMS 7
I.5.1 ONSHORE WIND FARMS 7
I.5.2 OFFSHORE WIND FARMS 8
I.6 WIND TURBINES 8
I.7 COMPONENTS OF WIND TURBINES 8
I.7.1 BLADES 8
I.7.2 ROTOR HUB 8
I.7.3 LOW SPEED SHAFT 8
I.7.4 GEAR BOX 8
I.7.5 HIGH SPEED SHAFT 9
I.7.6 ELECTRICAL GENERATOR 9
I.7.7 TURBINE TOWER 9
I.7.8 SENSORS AND BRAKES 9
I.8 CLASSIFICATION OF WIND TURBINES 10
I.8.1 HORIZONTAL AXIS WIND TURBINE 10
I.8.2 VERTICAL AXIS WIND TURBINE 12
I.9 AERODYNAMIC PERFORMANCE PARAMETERS 14
I.9.1 TIP SPEED RATIO (TSR) 14
I.9.2 POWER COEFFICIENT 14
I.9.3 TORQUE COEFFICIENT 15
I.9.4 LIFT COEFFICIENT 15

I.9.5 DRAG COEFFICIENT 15

CHAPTER II 17

II.1 INTRODUCTION 18
II.2 GEOMETRIC CHARACTERISTICS OF THE AIRFOIL SECTION 18
II.3 AERODYNAMIC FORCES ON A WIND TURBINE BLADE AIRFOIL 19
II.3.1 LIFT FORCE 19
II.3.2 DRAG FORCE 19
II.4 TYPES OF AIRFOILS IN WIND TURBINE BLADES 21
II.4.1 SYMMETRIC BICONVEX AIRFOILS 21
II.4.2 CONVEX-FLAT AIRFOILS 22
II.4.3 UNDERCAMBERED (HOLLOW) AIRFOILS 22
II.4.4 REFLEXED AIRFOILS 22
II.5 AIRFOILS FAMILIES 22
II.5.1 THE EARLY FOUNDATIONS (AVIATION ROOTS) 22
II.5.2 DEDICATED WIND TURBINE FAMILIES 23

CHAPTER III 26

III.1 INTRODUCTION 27
III.2 WIND TURBINE AERODYNAMIC THEORIES. 27
III.2.1 ACTUATOR DISC THEORY (AXIAL MOMENTUM THEORY) 27
III.2.2 BLADE ELEMENT THEORY (BET) 31
III.2.3 BLADE ELEMENT MOMENTUM (BEM) THEORY 33

CHAPTER IV 36

IV.1. INTRODUCTION 37
IV.2. DEFINITION OF QBLADE 37
IV.3. FUNCTIONALITIES OF QBLADE 37
IV.4. PRACTICAL STEPS FOR CONDUCTING A WIND TURBINE STUDY IN QBLADE 38
IV.5. VALIDATION OF THE NUMERICAL MODEL 43
IV.6. AERODYNAMIC PERFORMANCE COMPARISON OF CANDIDATE AIRFOILS 45
IV.7. THE AERO-STRUCTURAL TRADE-OFF AND PROPOSED HYBRID SOLUTION 46
IV.8. COMPARATIVE STRUCTURAL INTEGRITY AND AERODYNAMIC LOADING 47
IV.9. RESULTS 49

IV.9.1. STUDY OF THE EFFECT OF BLADE NUMBER 50
IV.9.2. STUDY OF THE EFFECT OF TIP SPEED RATIO 52
IV.9.3. STUDY OF THE EFFECT OF BLADE TIP RADIUS 54
IV.9.4. STUDY OF THE EFFECT OF ROTOR HUB RADIU 56
IV.9.5. STUDY OF THE EFFECT OF REYNOLDS NUMBER 58

GENERAL CONCLUSION ……..…….. 60

REFERENCES ……..…… 63

LIST OF FIGURES

CHAPTER I

Figure I. 1: Vertical wind speed profile (Wind Shear effect) 6
Figure I. 2: Weibull probability density function curves 7
Figure I. 3: Onshore wind farm 7
Figure I. 4: Offshore wind farm 8
Figure I. 5: Schematic diagram of a modern wind turbine configuration 9
Figure I. 6: Configuration of Upwind (left) and Downwind (right) 10
Figure I. 7: Three-bladed turbine (left) and multi-blade turbine (right) 11
Figure I. 8: Magnus effect turbine 11
Figure I. 9: Vertical Axis Wind Turbines (VAWT): 13

CHAPTER II

Figure II. 1: Main structural and aerodynamic characteristics of an airfoil profile 19
Figure II. 2: elocity triangle and aerodynamic forces acting on a blade element profile 21
Figure II. 3: Classification of aerodynamic airfoils based on geometric profiles 22
Figure II. 4: Profiles of various NACA 4-digit airfoil families 23
Figure II. 5: NREL S-series airfoils 24
Figure II. 6: Profiles of FFA (left) and RISØ (right) 24
Figure II .7: Profiles of Delft University (DU) 25

CHAPTER III

Figure III. 1: Wind energy extraction stream tube 27
Figure III. 2: Actuator disc stream-tube ..... **Erreur ! Signet non défini.**
Figure III. 3: Velocity distribution through a wind turbine ..... **Erreur ! Signet non défini.**
Figure III. 4: The variation in C_P and C_T with axial induction factor ..... **Erreur ! Signet non défini.**
Figure III. 5: Wind turbine blade divided into a series number of sections 31
Figure III. 6: Velocities on blade element 32
Figure III. 7: Flow chart of BEM theory 34

CHAPTER IV

Figure IV. 1: The Main Interface of QBlade Software 37

Figure IV. 2: Coordinates of the imported NACA4412 airfoil 38
Figure IV. 3: Distribution of Lift and Drag Coefficients and the Lift-to-Drag Ratio 39
Figure IV. 4: Power Coefficient Curve and Pressure Distribution 39
Figure IV. 5: 360° Polar Extrapolation Module.....40
Figure IV. 6: Design Module 40
Figure IV. 7: Rotor Simulation using Blade Element Momentum (BEM) Theory 41
Figure IV. 8: Multi-Parameter Simulation Module 42
Figure IV. 9: Turbulent Windfield Generator Module 42
Figure IV. 10: Free Wake Vortex Simulation Module 43
Figure IV. 11: Comparison of the aerodynamic efficiency between the current study and the reference study.....44
Figure IV. 12: Comparison of the power coefficient between the current study and the reference study.....45
Figure IV. 13: Comparison of aerodynamic efficiency.....45
Figure IV. 14: Comparison of power coefficient 46
Figure IV. 15: Blade structural model showing stress distribution in mixed blade.....48
Figure IV. 16: Blade structural model showing stress distribution in SG6043 only 48
Figure IV. 17: 3D rotor geometric models with varying blade numbers (NB = 3, 6, 12, 24).50
Figure IV. 18: Parametric performance curves (Power, Cp, Torque, Cm, Thrust, and Ct) as a function of blade number (NB).....51
Figure IV. 19: Parametric performance curves (Power, Cp, Torque, Cm, Thrust, and Ct).....53
Figure IV. 20: Parametric performance curves (Power, Cp, Torque, Cm, Thrust, and Ct).....55
Figure IV. 21: Parametric performance curves (Power, Cp, Torque, Cm, Thrust, and Ct).....57
Figure IV. 22: Parametric performance curves (Power, Cp, Torque, Cm, Thrust, and Ct).....59

NOMENCLATURE

Symbol	Description	Unit
C_p	Power Coefficient	[−]
C_D	Drag Coefficient	[−]
C_L	Lift Coefficient	[−]
ρ	Air Density	[kg/m3]
P_∞	Atmospheric Pressure (Ambient Pressure)	[Pa]
A_∞	Streamtube Inlet Cross-Sectional Area	[m2]
A_w	Streamtube Outlet Cross-Sectional Area	[m2]
A_d	Rotor Disc Area	[m2]
a	Axial Induction Factor	[−]
a′	Angular Induction Factor	[−]
V_{rel}	Relative Wind Velocity	[m/s]
ω	Angular Velocity of Airflow	[rad/s]
L	Aerodynamic Lift Force	[N]
D	Aerodynamic Drag Force	[N]
F_θ	Tangential Force Component	[N]
F_z	Axial Force Component (Thrust)	[N]
dQ	Elemental Torque	[N·m]
NB	Number of Blades	[−]
dr	Elemental Blade Radial Thickness	[m]
P	Rotor Mechanical Power Output	[W]
T	Thrust Force (Reaction Force)	[N]
σ	Local Blade Solidity Ratio	[−]

F or f	Prandtl's Loss Correction Factor (Tip/Root)	[−]
r	Local Radial Position along the Blade	[m]
M	Mach Number	[−]
E_{sys}	Total System Energy	[W]
W	Mechanical Work	[J]
F_{ext}	External Forces	[N]
dV	Control Volume Element	[m3]
C_t	Thrust Coefficient	[−]
TSR	Tip Speed Ratio	[−]
V_∞	Free-Stream Wind Velocity	[m/s]
V_d	Induced Velocity at the Rotor Disc	[m/s]
P_{in}	Pressure at the Streamtube Inlet	[Pa]
P_d	Static Pressure at the Rotor Disc	[Pa]
P_w	Static Pressure at the Streamtube Wake	[Pa]
SC	Control Surface Area	[m2]
ϕ	Relative Flow Angle	[deg]
β	Blade Pitch Angle (Twist Angle)	[deg]
α	Angle of Attack (AoA)	[deg]

General introduction

GENERAL INTRODUCTION

The contemporary world is undergoing a rapid, paradigm shift toward clean and sustainable energy technologies, driven by the continuous depletion of global fossil fuel reserves and the critical environmental challenges posed by greenhouse gas emissions and climate change. Within this framework, renewable energy sources have emerged as an inevitable strategic alternative to guarantee global energy security and achieve sustainable development. Among these alternatives, wind energy occupies a pioneering position, recognized as one of the most mature, efficient, and economically viable technologies in the global power market, operating through both utility-scale wind farms and localized, decentralized micro-generation systems.

Developing efficient wind energy conversion systems requires a progressive engineering approach. This methodology begins with a solid technological overview, moves through the hydrodynamic analysis of blade sections, establishes governing mathematical frameworks, and culminates in advanced computational simulations and validation.

Problem Statement and Research Objectives: The core engineering problem addressed in this thesis is how to design a small-scale wind turbine rotor that achieves maximum aerodynamic efficiency and power extraction while maintaining structural integrity under low Reynolds number, highly turbulent flow conditions. To address this issue, this research work conducts a comprehensive investigation evaluating the influence of critical geometric parameters on rotor performance, utilizing an aerodynamic optimization strategy that deploys a hybrid layout of specialized airfoils to balance aerodynamic lift and structural stress distribution.

To systematically address this problem and establish the scientific foundation of this study, the thesis is organized into four interconnected chapters as follows:

Chapter I: GENERAL OVERVIEW OF WIND TURBINES: This chapter establishes a comprehensive foundational introduction to wind energy systems. It details the historical evolution, classifications, and operating principles of wind turbines, while providing an in-depth exploration of their primary technological components and electromechanical subsystems.

Chapter II: AERODYNAMIC FOUNDATIONS OF WIND TURBINE BLADES: This chapter focuses on the fluid dynamics governing the cross-sectional profiles (airfoils) of the blades. It analyzes the physics of lift and drag forces, evaluates the aerodynamic characteristics of specific airfoil families, and provides the engineering rationale behind the selection of the mixed and optimized airfoil profiles utilized in the current design.

Chapter III: AERODYNAMIC MODELING AND PERFORMANCE THEORIES: This chapter serves as the mathematical and theoretical backbone of the thesis. It details the fluid dynamic theories governing energy extraction across the rotor, starting from the classical Actuator Disk Theory and the theoretical Betz Limit, progressing through the Blade Element Theory (BET), and culminating in the unified mathematical framework of the Blade Element Momentum (BEM) theory along with its essential engineering correction factors.

Chapter IV: PARAMETRIC STUDY OF A SMALL WIND TURBINE USING QBLADE SOFTWARE: This chapter represents the practical and numerical core of the research work. It utilizes the dedicated simulation software QBlade to model the optimized rotor architecture, validate the numerical results against established reference literature, conduct an extensive parametric study evaluating the impact of geometric variables, and execute a structural analysis to assess Von Mises stress propagation and design viability.

By bridging the gap between aerodynamic theory and numerical simulation, this investigation aims to contribute actionable engineering insights toward optimizing the performance, reliability, and deployment of small-scale wind energy systems.

Chapter I
GENERAL OVERVIEW

I.1 Introduction

The global energy sector is facing a change to be more sustainable. As we use up fuels Renewable Energy is becoming the main way to make sure we have energy for a long time and to protect the environment. Renewable Energy sources are a way to get power and we will never run out of them so they are changing how we make electricity all over the world.

One of the alternatives is Wind Energy. It is a good way to make electricity and it does not hurt the environment. Wind Energy works by using the energy in the air and turning it into power. This is an important part of the global energy sector. This part of the book looks at the basics of Wind Energy like what it's how it helps us get closer to using carbon-neutral power. We will explore how Wind Energy is a part of the global energy mix and why it is so important, for our future.

I.2 Overview of Wind Energy

I.2.1 Definition of Wind

Wind results from the movement of air due to atmospheric pressure gradients. Wind flows from regions of higher pressure to regions of lower pressure. The larger the atmospheric pressure gradient, the higher the wind speed and thus, the greater the wind power that can be captured from the wind by means of wind energy-converting machinery. The generation and movement of wind are complicated due to a number of factors. Among them, the most important factors are uneven solar heating, the Coriolis effect due to the earth’s self-rotation, and local geographical conditions. [1]

I.2.2 Wind Energy concept

Wind energy is defined as the harnessed kinetic energy of air in motion, resulting from the atmospheric pressure differences. From an engineering standpoint, it is the process of extracting the mechanical power available in the wind stream and converting it into a usable form, such as electricity. This conversion is governed by the laws of fluid mechanics and thermodynamics, specifically limited by the Betz Law, which defines the maximum theoretical efficiency that a wind turbine can achieve in capturing the energy of the moving air. [2]

I.3 Wind Energy conversion chain

I.3.1 Kenetic to mechanical

Kinetic wind energy is converted to mechanical energy by the aerodynamic design of wind turbine rotor blades (airfoils) interacting with moving air. As the air passes over the rotor blade surface, it creates pressure differences from one side of the blade to the other, creating a lift force that causes the rotor to turn; thus, converting the linear motion of air molecules into organized rotational motion, generating torque at the rotor hub. The generated mechanical power is then transmitted through the main shaft of the wind turbine, ultimately producing rotational kinetic energy available for use.

I.3.2 Mechanical to electrical

Generators serve to convert mechanical energy to electrical energy, primarily using Faraday's Law, which states that a change in magnetic flux relative to a conducting material will produce an electromotive force (EMF). When the turbine shaft rotates, it turns the generator

rotor, which contains magnets or electromagnets, producing a variance in the magnetic flux relative to the stationary copper coils that make up the generator stator. In this manner, as magnetic flux changes across the coils of the stator, a current is induced, causing electrons to flow through the coils and producing an alternating current (AC). Thus, in the final step of this energy transformation chain, the mechanical work supplied to the generator rotor overcomes magnetic forces and is converted into electrical energy.

I.4 Wind Energy potential

I.4.1 Vertical wind speed gradient

The Vertical Wind Speed Gradient (VWSG), also known as Wind Shear, is a meteorological phenomenon in which wind increases with the height above the ground. The effect of height on the wind speed is mainly due to roughness on the earth's surface and can be estimated using the Hellmann power equation that relates wind speeds at two different heights:

$$v = v_{ref}\left(\frac{h}{h_{ref}}\right)^{\alpha} \qquad (I.1)$$

α is the wind shear coefficient. In practice, α depends on a number of factors, including the roughness of the surrounding landscape, height, time of day, season, and locations. The wind shear coefficient is generally lower in daytime and higher at night. Empirical results indicate that wind shear often follows the "1/7 power law". The values of wind shear coefficient for different surface roughness. Because the power output of wind turbine strongly depends on the wind speed at the hub height, modern wind turbines are built at the height greater than 80 m, for capturing more wind energy and lowering cost per unit power output (figure I.1). [3]

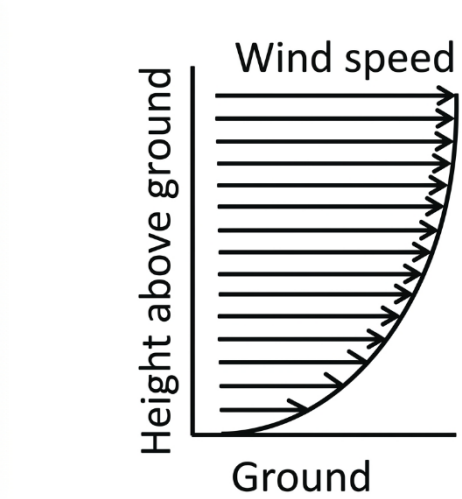


Figure I. 1: Vertical wind speed profile (Wind Shear effect)

I.4.2 Weibull distribution

The Weibull Distribution is the standard statistical tool used in wind engineering to characterize the frequency and variability of wind speeds at a particular location over time. Unlike the vertical wind speed gradient, which describes spatial change (height), the Weibull model provides a temporal probability profile. It allows engineers to move beyond simple averages and understand how often the wind blows at specific speeds, which is essential for

calculating the Annual Energy Production (AEP). Since wind power is proportional to the cube of the velocity, the distribution's "tail" (representing high-speed wind events) often holds the most significant energy potential, even if those speeds occur less frequently.

The probability of the wind blowing at a specific velocity is given by the Probability Density Function (figure I.2): [4]

$$f(v) = \frac{k}{C}\left(\frac{v}{C}\right)^{k-1} \exp\left[-\left(\frac{v}{C}\right)^{k}\right] \qquad (I.2)$$

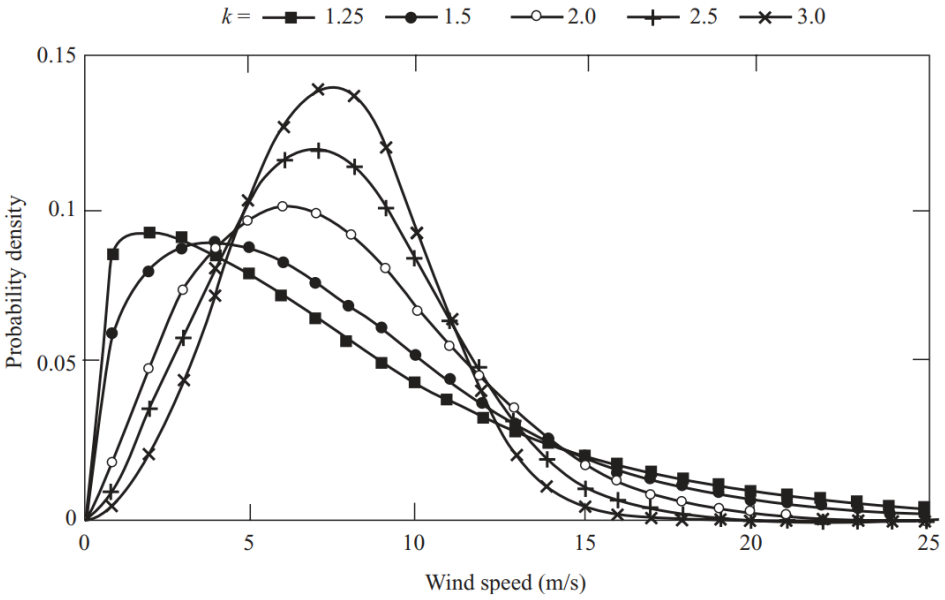


Figure I. 2: Weibull probability density function curves for different shape parameters (k)

I.5 Classification of wind farms

I.5.1 Onshore wind farms

Onshore wind farms refer to wind turbine installations located on land, characterized by low cost, easy maintenance, and straightforward interconnection to the electrical grid. They are suitable for countries with large areas that have desired wind speeds (figure I.3).



Figure I. 3: Onshore wind farm

I.5.2 Offshore wind farms

In contrast, offshore wind refers to facilities located offshore, generally several miles from the coast. They benefit from stronger and more consistent winds, increasing energy production and reducing visual and noise impacts on inhabited areas (figure I.4).



Figure I. 4: Offshore wind farm

I.6 Wind turbines

A wind turbine is defined as a device that converts the kinetic energy of wind into electrical energy, typically rotating around a horizontal or vertical axis, with the design optimized to efficiently exploit wind speed. Wind turbines can be installed onshore or offshore, with each location offering unique design characteristics and economic considerations. [5]

I.7 Components of wind turbines

I.7.1 Blades

Their mission is to harness the kinetic energy carried by the wind to rotate the low-speed shaft, which is connected to the blades via the rotor hub.

I.7.2 Rotor hub

Located at the front of the turbine, it is connected to the low-speed shaft on one side while the blades rest on its sides. Its primary function is to rotate with the blades and drive the low-speed shaft; it also provides support and connection for the blades.

I.7.3 Low Speed Shaft

It is connected to the blades through the rotor hub and rotates at the same speed as the blades. Its task is to transmit motion to the gearbox.

I.7.4 Gear Box

The gearbox consists of a set of interlocking gears. Large gears are located on the side of the low-speed shaft, while smaller gears are on the side of the high-speed shaft. The goal is to transmit motion and increase the speed so that it becomes suitable for the electrical generator's rotational speed.

I.7.5 High Speed Shaft

It is connected to the gearbox on one side and to the electrical generator on the other. Its task is to transmit motion from the gearbox to the electrical generator.

I.7.6 Electrical Generator

The electrical generator is connected to the high-speed shaft and rotates to generate electrical energy. Wires exit the generator and pass through the turbine tower to reach a transformer, whose task is to increase the electrical voltage value. The latter is connected to a substation that links several turbines together and ensures the connection to the electrical grid, thereby transmitting the produced energy to the grid.

I.7.7 Turbine Tower

The tower is designed to support the entire weight of the turbine body. Inside, wires from the generator pass down to the transformer. Ladders are also built inside the tower so maintenance workers can reach the turbine sections when needed. The base of the tower includes a control room to monitor turbine performance and stop it during maintenance, for example. An electrical transformer may be located at the base or outside. At the top of the tower, at the point of contact with the turbine body, there is a yaw motor connected to a computer that analyzes signals coming from the sensors and subsequently sends a signal to the motor to rotate the turbine body to face the wind direction (figure I.5).

I.7.8 Sensors and Brakes

A sensor is located at the end of the turbine body to monitor wind direction and speed, positioned away from the influence of the wind hitting the blades. The sensor is connected to a computer that constantly receives information about wind speed and direction; the computer analyzes these signals and sends a command to the yaw motor to correct the turbine's orientation. As for the brakes, they are located on the shafts, and their mission is to stop the rotation of the turbine when needed for maintenance or during severe storms to ensure turbine protection.

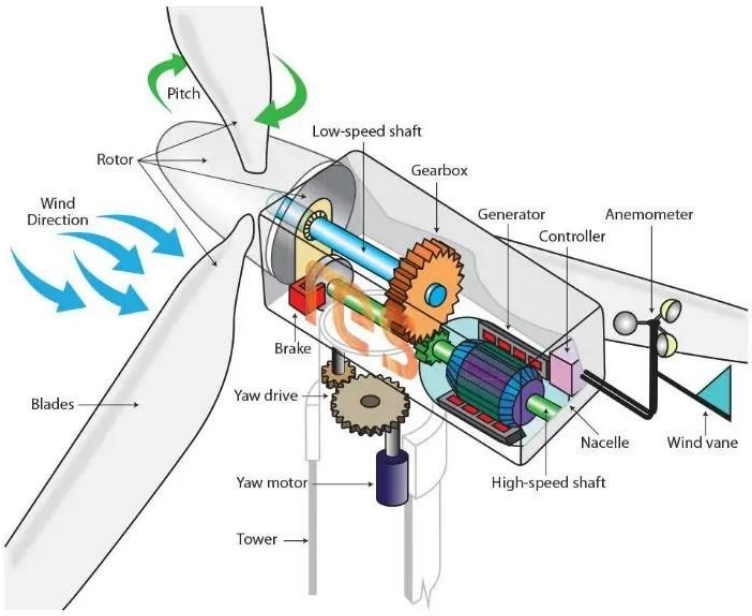


Figure I. 5: Schematic diagram of a modern wind turbine configuration

I.8 Classification of wind turbines

I.8.1 Horizontal Axis Wind Turbine

A Horizontal Axis Wind Turbine (HAWT) is the most common type of wind turbine used today for large-scale power generation. Its defining characteristic is that the main rotor shaft and electrical generator are positioned horizontally at the top of a tower, and the blades must be pointed into the wind to generate power [6]. There are several types, most notably :

- Upwind turbines: the rotor is positioned on the windward side of the tower, meaning the blades face the wind directly before it reaches the tower structure. This design requires an active yaw system to keep the rotor oriented into the wind but is the industry standard due to its higher aerodynamic efficiency and reduced turbulence compared to downwind designs.
- Downwind turbines: the rotor is positioned on the leeward side of the tower, meaning the wind passes the tower structure before hitting the blades. Unlike upwind models, these turbines are often designed to be "self-aligning," naturally following the wind direction like a weather vane, which can reduce the need for a complex active yaw system (figure I.6).

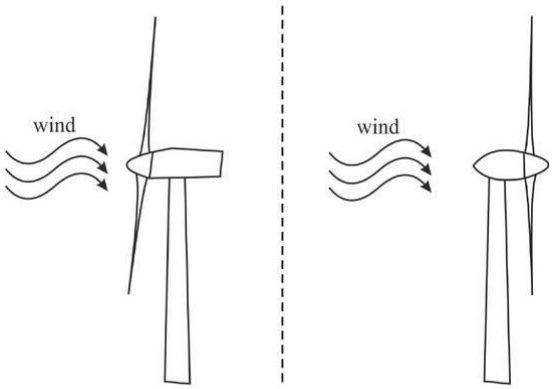


Figure I. 6: Configuration of Upwind (left) and Downwind (right) horizontal axis wind turbines

- Three-bladed turbines: the standard configuration for modern wind energy, featuring a rotor with three aerodynamic blades mounted on a horizontal axis. This design is preferred because it offers an optimal balance between high aerodynamic efficiency and structural stability; specifically, the three-blade arrangement provides a constant moment of inertia during rotation, which minimizes gyroscopic vibration and mechanical stress on the turbine's drive train and hub compared to one or two-bladed designs.
- Multi-blade turbines: is a high-solidity rotor configuration featuring a large number of blades (typically 12 to 40) designed to produce high starting torque at low wind speeds. Unlike modern turbines used for electricity, these are primarily utilized for mechanical tasks, such as water pumping, because their high surface area allows them to overcome

heavy initial loads, even though they operate at much lower rotational speeds and aerodynamic efficiencies (figure I.7).

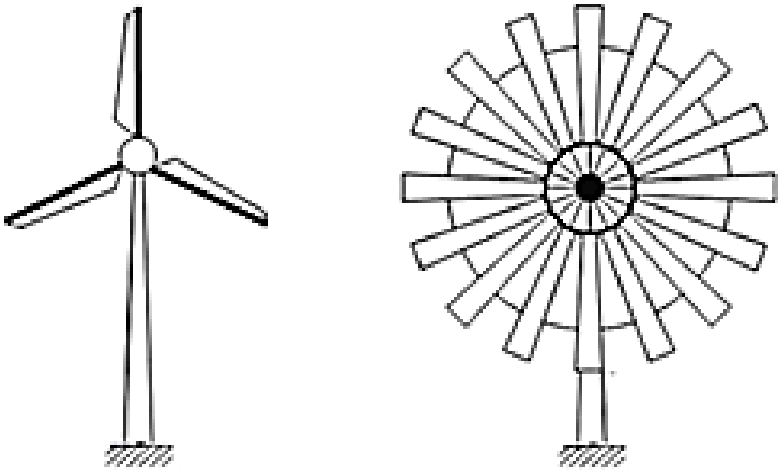


Figure I. 7: Three-bladed turbine (left) and multi-blade turbine (right)

- Magnus Effect Turbine: is a type of wind turbine that replaces traditional airfoil blades with rotating cylinders. It generates lift through the Magnus Effect, where the rotation of the cylinders in a moving air stream creates a pressure differential-similar to a spinning ball curving through the air. This design allows the turbine to operate efficiently in high or turbulent wind conditions where traditional blades might stall, and it offers better control over rotational speed by simply adjusting the spin rate of the cylinders (figure I.8).

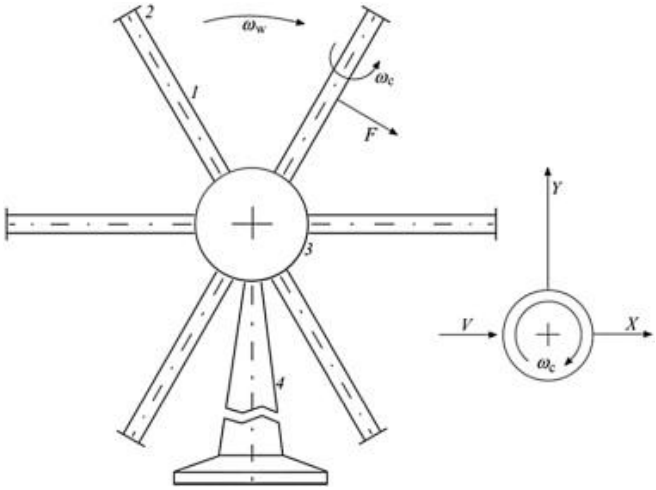


Figure I. 8: Magnus effect turbine

Although various types exist, they largely converge in terms of their primary advantages and disadvantages, as outlined below:

Advantages:

- ☑ High Aerodynamic Efficiency: HAWT blades are designed as airfoils that utilize lift rather than drag. This allows the blades to move faster than the wind itself (High Tip-Speed Ratio), resulting in much higher energy extraction efficiency compared to vertical axis models.

- ☑ Vertical Wind Speed Gradient (VWSG) Access: Because HAWTs are mounted on tall towers, they reach higher altitudes where wind is faster and less turbulent. Since power is proportional to the cube of the wind speed, even a small increase in height leads to a massive increase in power output.
- ☑ Pitch and Yaw Control: Modern HAWTs can adjust the angle of their blades (Pitching) and the direction of the nacelle (Yawing). This allows them to maximize energy capture in varying wind conditions and protect the structure by "feathering" the blades during extreme storms.
- ☑ Self-Starting Capability: Unlike some vertical axis designs that require an external motor to begin spinning, the airfoil design of HAWT blades allows them to start rotating automatically once the wind reaches the "cut-in" speed.
- ☑ Scalability: The horizontal configuration is well-suited for massive scales. Modern offshore HAWTs can have rotor diameters exceeding 200 meters, allowing a single turbine to produce enough electricity for thousands of homes.

Disadvantages:

- ☒ Structural and Weight Constraints: Because the Generator and Gearbox are located at the top of the tower (within the nacelle), the tower must be exceptionally strong to support this heavy mass. This increases material costs and complicates the engineering of the foundation.
- ☒ Maintenance Challenges: Since the main mechanical and electrical components are housed at a great height, maintenance is difficult and expensive. It requires specialized cranes and technicians to climb the tower or use external platforms to access the High-Speed Shaft and generator.
- ☒ Yaw System Requirement: Unlike vertical axis turbines, HAWTs cannot capture wind from all directions automatically. They require a complex Yaw System (motors, sensors, and bearings) to rotate the entire nacelle, adding another point of potential mechanical failure.
- ☒ Installation Logistics: The massive size of the Blades and tower sections makes transportation and assembly a major logistical hurdle, especially in remote areas or rugged terrain.
- ☒ Cyclic Loading and Fatigue: As previously discussed, the Vertical Wind Speed Gradient causes the blades to experience different forces as they rotate. This Cyclic Loading leads to material Fatigue, which can shorten the operational life of the rotor hub and blades if not managed correctly.

I.8.2 Vertical Axis Wind Turbine

A Vertical Axis Wind Turbine (VAWT) is a type of wind turbine where the main rotor shaft is set transversely to the wind (usually vertically) while the main components are located at the base of the turbine. This orientation allows the generator and gearbox to be placed at ground level for easier maintenance and enables the turbine to capture wind from any direction (360°) without the need for a yaw mechanism [7]. This category comprises three primary types (figure I.9):

- Savonius turbines: is a drag-based vertical axis wind turbine (VAWT) characterized by two or more semi-cylindrical scoops (S-shaped cross-section) that catch the wind. Because it relies on aerodynamic drag rather than lift, it produces high starting torque at low wind speeds making it ideal for self-starting, but operates at lower rotational speeds and lower overall efficiency compared to lift-based turbines.
- Darrieus turbines: is a lift-based vertical axis wind turbine (VAWT) characterized by curved, airfoil-shaped blades connected to a central rotating shaft, often resembling an eggbeater. Unlike the Savonius model, it utilizes aerodynamic lift to achieve high rotational speeds and greater efficiency; however, it typically lacks self-starting capability and requires an external power source or a secondary starter motor to reach its operational velocity.
- H-Rotor Turbine (or Giromill): is a vertical axis wind turbine (VAWT) featuring straight, vertical airfoil blades attached to a central shaft by horizontal arms. As a variation of the Darrieus design, it utilizes aerodynamic lift to achieve high efficiency, but its straight-blade configuration is simpler to manufacture and often incorporates pitch control mechanisms to improve self-starting capabilities and structural stability.

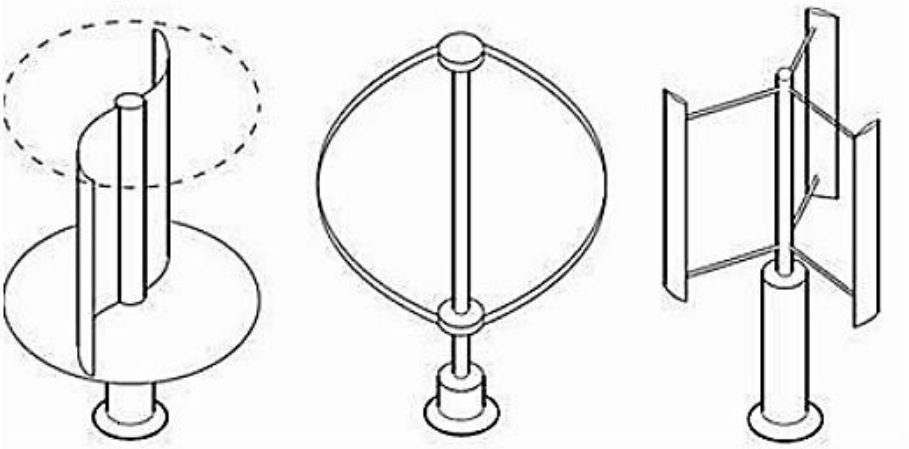


Figure I. 9: Vertical Axis Wind Turbines (VAWT):
Savonius, Darrieus, and H-Rotor (Giromill)

The advantages and disadvantages of Vertical Axis Wind Turbines (VAWT) center on their mechanical simplicity and suitability for complex wind environments:

Advantages:

- ☑ Omni-directional Capability: VAWTs can capture wind from any direction 360° without requiring a Yaw System. This simplifies the design and allows for instantaneous response to frequent changes in wind direction.
- ☑ Ground-Level Components: The Generator, Gearbox, and heavy electrical components are located at the base of the tower. This significantly reduces the structural load on the tower and makes maintenance much safer and more cost-effective, as technicians do not need to climb to great heights.
- ☑ Performance in Turbulent Wind: They are more effective than HAWTs in urban environments or rugged terrain where the wind is often turbulent and "gusty" rather than smooth and laminar.

- ☑ Lower Noise Profile: Because they generally operate at lower tip-speed ratios, they produce less aerodynamic noise, making them more suitable for residential or small-scale applications.
- ☑ Compact Footprint: VAWTs can be placed closer together in wind farms because they are less affected by the "wake effect" (turbulence created by an upstream turbine) compared to horizontal models.

Disadvantages:

- ☒ Lower Aerodynamic Efficiency: Most VAWT designs (especially drag-based ones like the Savonius) have a lower Power Coefficient than horizontal turbines, meaning they extract less energy from the same amount of wind.
- ☒ Self-Starting Issues: Many lift-based VAWTs (like the Darrieus) cannot start rotating on their own from a standstill and require an external motor or a hybrid Savonius-starter to reach operational speeds.
- ☒ Pulsating Torque: As the blades rotate, the angle of attack changes constantly relative to the wind. This creates "torque ripple" or pulsating forces that can lead to mechanical fatigue and vibration in the drive train.
- ☒ Lower Wind Speeds: Because they are often shorter than HAWTs, they cannot access the higher, more consistent wind speeds found at greater altitudes (missing the benefits of the Vertical Wind Speed Gradient).
- ☒ Guy-Wire Requirements: Many large VAWTs require support cables (guy-wires) to stay upright, which increases the ground space required for installation and adds mechanical complexity to the site.

I.9 Aerodynamic performance parameters

I.9.1 Tip Speed Ratio (TSR)

Tip Speed Ratio (TSR) is a dimensionless aerodynamic parameter defined as the ratio between the tangential speed of the blade tips and the actual velocity of the free-stream wind. It is calculated using the formula:

$$\lambda = \frac{\omega R}{v} \qquad (I.3)$$

The TSR is a fundamental factor in determining a wind turbine's efficiency (Power Coefficient, C_p); an optimal ratio ensures that the blades rotate at a speed that maximizes wind interception while minimizing aerodynamic interference and turbulence.

I.9.2 Power Coefficient

Power Coefficient (C_p) is defined as a dimensionless measure of a wind turbine's aerodynamic efficiency, representing the ratio of the mechanical power extracted by the rotor to the total kinetic power available in the wind stream intersecting its swept area. Mathematically, it is expressed as:

$$C_p = \frac{P_{extracted}}{P_{wind}} = \frac{P}{\frac{1}{2}\rho A v^3} \qquad (I.4)$$

This coefficient is governed by the Betz Limit, which establishes a theoretical maximum efficiency of 59.3%. In practice, the actual C_p value is primarily a function of the Tip Speed Ratio (TSR) and the blade pitch angle. Modern high-performance turbines are engineered to achieve peak C_p values ranging from 0.45 to 0.50 to optimize energy harvesting.

I.9.3 Torque Coefficient

The Torque Coefficient (C_m or C_t) is a dimensionless aerodynamic parameter that characterizes the capacity of a wind turbine rotor to generate rotational torque relative to the dynamic pressure of the wind and the rotor's physical dimensions. It is analytically defined by the expression:

$$C_m = \frac{T}{\frac{1}{2}\rho A R v^2} \qquad (I.5)$$

This coefficient serves as a critical metric for evaluating the self-starting capabilities and structural load profiles of various turbine architectures. Furthermore, it maintains a fundamental mathematical correlation with the Power Coefficient (C_p) through the Tip Speed Ratio (λ), expressed as:

$$C_p = C_m \cdot \lambda \qquad (I.6)$$

While drag-based configurations like the Savonius rotor exhibit high C_m values at low speeds facilitating superior starting torque, lift-based systems typically optimize C_m to achieve higher power extraction efficiencies at elevated operational velocities.

I.9.4 Lift Coefficient

Lift Coefficient (C_L) is a dimensionless aerodynamic parameter that quantifies the lift force generated by an airfoil or turbine blade relative to the dynamic pressure of the fluid flow and the blade's planform area. It is analytically expressed by the following governing equation:

$$C_L = \frac{2L}{\rho A v^2} \qquad (I.7)$$

In the context of wind energy conversion systems, C_L is a fundamental function of the Angle of Attack (α). It exhibits a linear increase within the laminar flow regime until reaching a critical threshold known as the Stall Point, where flow separation leads to a significant reduction in lift and a concomitant increase in drag.

I.9.5 Drag Coefficient

Drag Coefficient (C_D) is a dimensionless aerodynamic parameter that quantifies the total resistance force exerted on an airfoil or turbine blade relative to the dynamic pressure of the oncoming flow and the blade's projected reference area. It is analytically defined by the following governing equation:

$$C_D = \frac{2D}{\rho A v^2} \qquad (I.8)$$

In wind turbine analysis, C_D serves as a critical indicator of aerodynamic inefficiency for lift-based rotors, as it represents the parasitic retarding force that opposes the torque-generating lift. Conversely, for drag-based architectures such as the Savonius rotor, the optimization of C_D is the primary objective for rotational momentum. The coefficient is highly non-linear and sensitive to the Angle of Attack (α), exhibiting a substantial increase upon the onset of flow separation at the Stall Point, where laminar flow transitions into a turbulent wake.

Chapter II
AERODYNAMIC FOUNDATIONS OF WIND TURBINES BLADE

II.1 Introduction

While energy analysis is fundamental to wind turbine theory, it cannot yield a comprehensive design without a precise geometric study of the blade. Geometry serves as the functional medium translating physical laws into aerodynamic performance. Key parameters, including airfoil selection, chord distribution, and twist angles, govern the interaction between the structure and airflow. These characteristics dictate lift and drag coefficients, determining energy extraction efficiency. Thus, investigating geometric specifications is essential for optimizing performance, forming the primary focus of this chapter.

II.2 Geometric Characteristics of the Airfoil Section

- **Chord Length (C):** The fundamental reference baseline, defined as the straight-line distance connecting the leading edge to the trailing edge.
- **Leading Edge:** The foremost point of the airfoil section in a two-dimensional (2D) plane, or the foremost continuous line of the blade in a three-dimensional (3D) configuration, representing the initial point of contact with the incoming airflow.
- **Trailing Edge**: The rearmost point in a 2D section, or the rearmost line in a 3D configuration, where the airflow passing over the upper and lower surfaces recombines.
- **Suction Side (Extrados):** The uppermost boundary of the airfoil profile, typically characterized by a convex curvature.
- **Pressure Side (Intrados):** The lowermost boundary of the airfoil profile, which generally exhibits a concave shape or a lesser degree of convexity compared to the upper surface.
- **Mean Camber Line:** The geometric locus of points located exactly midway between the upper and lower surfaces, formally defined as the centers of inscribed circles tangent to both surfaces along the profile [8].
- **Thickness (e) and Maximum Thickness (e_{max}):** The thickness represents the diameter of the inscribed tangent circles, measured as the perpendicular distance to the chord line between the upper and lower surfaces. The maximum thickness (e_{max}) is the largest vertical measurement between these two surfaces along the entire chord [8].
- **Maximum Camber (f_{max}):** The maximum perpendicular displacement measured from the chord line to the mean camber line.
- **Relative Thickness:** A crucial dimensionless aerodynamic parameter representing the ratio of the maximum thickness to the chord length:

$$Relative\ Thickness = \frac{e_{max}}{C} \qquad (II.1)$$

- **Relative Camber:** A dimensionless ratio comparing the maximum camber displacement to the total chord length:

$$Relative\ Camber = \frac{f_{max}}{C} \qquad (II.2)$$

- **Relative Leading-Edge Radius:** The dimensionless ratio of the leading-edge radius of curvature to the total chord length:

$$RLER = \frac{r_{LE}}{C} \qquad (II.3)$$

- **Relative Trailing-Edge Radius:** The dimensionless ratio of the trailing-edge radius of curvature to the total chord length:

$$RTER = \frac{r_{TE}}{C} \qquad (II.4)$$

- **Leading-Edge Angle (φ_1):** The geometric angle formed between the chord line and the tangent to the mean camber line at the leading edge.
- **Trailing-Edge Angle (φ_2):** The geometric angle formed between the chord line and the tangent to the mean camber line at the trailing edge.
- **Camber Angle (φ):** The overall angular deflection of the mean camber line, representing the angular difference between the leading-edge and trailing-edge angles (φ_1 and φ_2).
- **Blade Span (h):** The total longitudinal macro-dimension, representing the distance measured from the root of the blade to its tip (figure II.1).

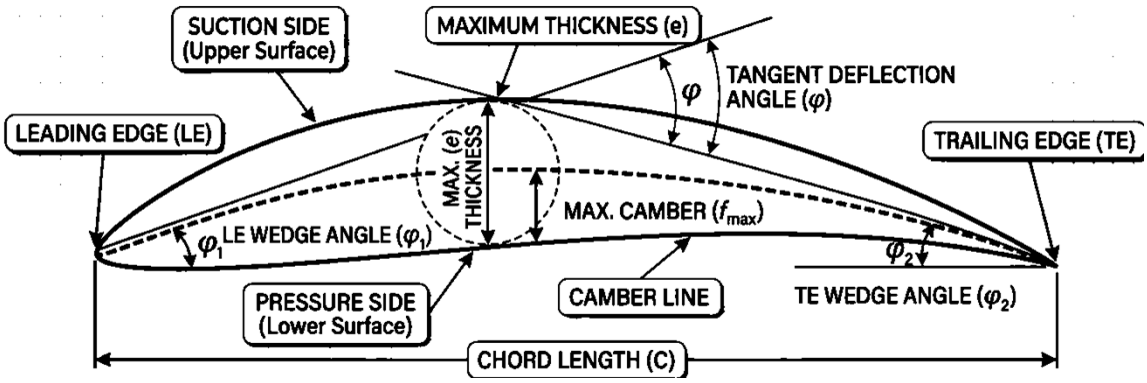


Figure II. 1: Main structural and aerodynamic characteristics of an airfoil profile

II.3 Aerodynamic forces on a wind turbine blade airfoil

II.3.1 Lift Force

Lift, upward-acting force on an aircraft wing or airfoil. An aircraft in flight experiences an upward lift force, as well as the thrust of the engine, the force of its weight, and a drag force. The lift force arises because there is a zone of low air pressure on the top of the airfoil and a zone of high pressure on the bottom of the airfoil caused by the flow of air over the airfoil [9].

II.3.2 Drag Force

The force of drag on an object when it is moving in a fluid (either a gas or a liquid). You feel the drag force when you move your hand through the water. You might also feel it if you move your hand during a strong wind. The faster you move your hand, the harder it is to move. You feel a smaller drag force when you tilt your hand so only the side goes through the air, you have decreased the area of your hand that faces the direction of motion. Like friction, the drag

force always opposes the motion of an object. Unlike simple friction, the drag force is proportional to some function of the velocity of the object in that fluid [10]. Mathematically:

$$F_D \propto \upsilon^2 \qquad (II.5)$$

$$F_D = \frac{1}{2} C_D \rho A v^2 \qquad (II.6)$$

Where C_D is the drag coefficient, A is the area of the object facing the fluid, and ρ is the density of the fluid.

As air flows around the wind turbine blade airfoil, the airfoil extracts a portion of the kinetic energy of the airflow due to the variation in flow velocity between its upper and lower surfaces. The airflow velocity is higher over the upper surface (suction side) and lower over the lower surface (pressure side). According to Bernoulli's principle, an increase in flow velocity results in a decrease in pressure on the upper surface, while the lower velocity on the lower surface leads to an increase in pressure. This pressure difference generates aerodynamic forces acting on the airfoil.

These aerodynamic forces mainly consist of the drag force $\overrightarrow{F_D}$, which acts parallel to the relative airflow velocity and opposes the motion, and the lift force $\overrightarrow{F_L}$, which acts perpendicular to the relative airflow velocity. The lift force is primarily responsible for converting the kinetic energy of the wind into rotational mechanical energy that drives the turbine rotor.

In practice, the blade section moves along a circular path within the rotating rotor plane. The resultant aerodynamic force $\vec{R}$ is obtained from the vector combination of the lift and drag forces. By projecting this resultant force onto the tangential direction of rotation, the tangential component $\overrightarrow{F_u}$ is obtained, which is responsible for generating the torque required to rotate the turbine.

Furthermore, V_θ represents the tangential velocity associated with blade rotation, while V_d denotes the axial wind velocity entering the rotor. Together with the relative velocity V_{rel}, these velocities form the velocity triangle used to define the different aerodynamic angles, as illustrated in the figure.

So, we have these two velocities that make up the velocity triangle. This triangle helps us understand some angles.:

- **Angle of Attack (α):** is the angle between the airfoil chord line and the relative velocity vector.
- **Twist Angle (β):** is the angle between the chord line and the plane that the airfoil is rotating in.
- **Relative Flow Angle (φ):** is the angle, between the plane that the airfoil is rotating in and the relative velocity vector.

These angles are related by the expression:

$$\varphi = \beta + \alpha \qquad (II.7)$$

To figure out how the wind turbine works we need to know the speed of the air and the angle at which it hits the blades. This is really important for the rotor and it affects how much power the wind turbine can make. The velocity field and the local angles of attack along the blade span are crucial for this. We have to get this right to understand the loading, on the rotor and the resulting power output of the wind turbine (figure II.2).

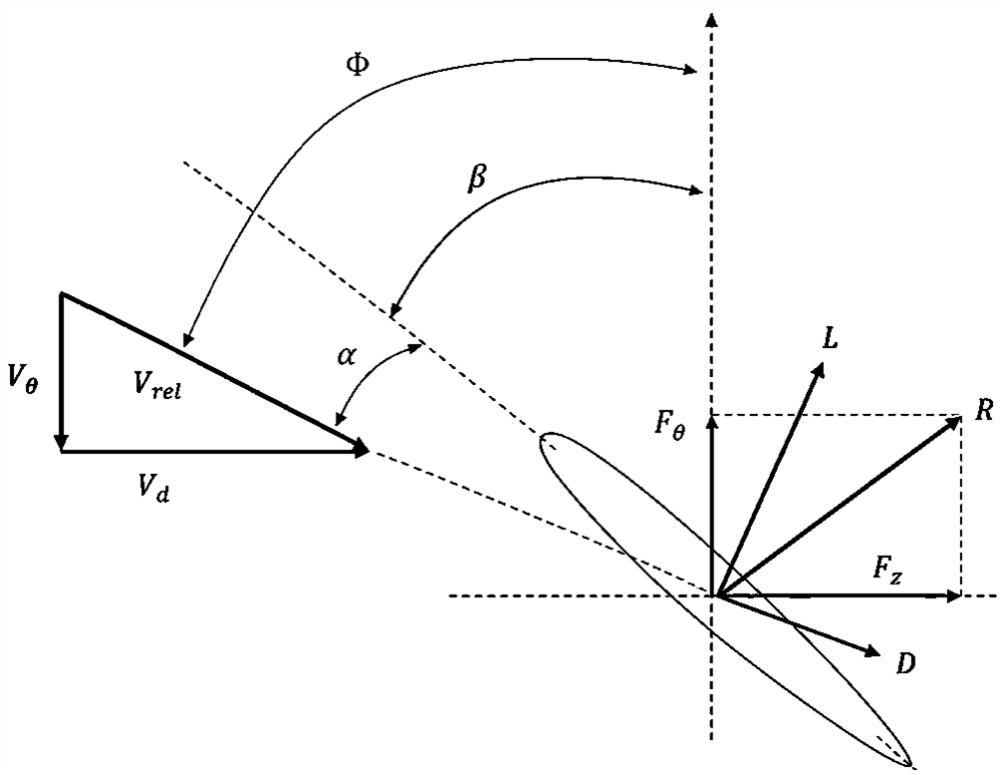


Figure II. 2: elocity triangle and aerodynamic forces acting on a blade element profile

The aerodynamic forces (lift and drag) acting on any given blade section are governed principally by the local relative velocity, the angle of attack, the physical properties of the fluid flow, the blade geometry, and the wake effect, which generates an induced velocity at each radial station. This induced velocity is essentially the manifestation of the aerodynamic loading distributed along the blades, thereby altering the effective angle of attack experienced by each cross-section.

As the blade encounters the relative airflow, viscous boundary layers develop along its suction and pressure surfaces, merging at the trailing edge to form the wake. Experimental studies of flow over fixed (non-rotating) wings reveal the generation of edge vortices (designated as secondary vortices) that are convected downstream, significantly altering the aerodynamic loading on the blade. In rotating systems, the intensity of these vortical structures attenuates with increasing radial distance from the hub, adopting a distinct helical configuration as they trail into the downstream flow [6].

II.4 Types of airfoils in wind turbine blades

II.4.1 Symmetric biconvex airfoils

exhibit camber symmetry about the chord line, with both upper and lower surfaces presenting convex curvature of roughly equal magnitude. This geometry yields identical aerodynamic responses under positive and negative angles of attack.

II.4.2 Convex-flat airfoils

combine a distinctly curved upper surface with a completely planar lower surface. This configuration generates favorable pressure gradients on the suction side, providing better lift characteristics than symmetric profiles at moderate incidence angles.

II.4.3 Undercambered (hollow) airfoils

feature a convex upper surface paired with a concave lower surface. The pronounced camber accentuates the velocity differential between pressure and suction sides, though this design typically incurs higher viscous drag penalties.

II.4.4 Reflexed airfoils

display an inflected camber line where the curvature reverses direction near the trailing edge transitioning from convex-upper/concave-lower at the leading portion to concave-upper / convex-lower at the rear. This S-shaped geometry offers inherent pitch stability by shifting the aerodynamic center aftward (figure II.3).

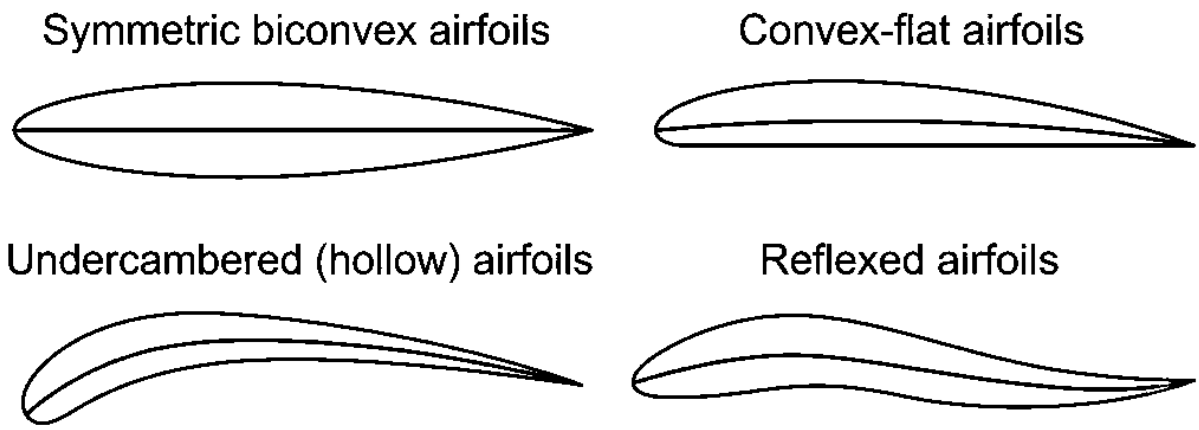


Figure II. 3: Classification of aerodynamic airfoils based on geometric profiles

II.5 Airfoils families

Wind turbine blades operate under completely different conditions than aircraft wings. While planes are built for high speed and keeping drag to an absolute minimum, wind turbines have a different job: they need to maximize torque at lower speeds, handle high angles of attack without stalling abruptly, and withstand intense structural loads especially down near the root.

To handle these conflicting demands, a modern blade doesn't just use one shape. It uses a blend of different airfoil families, transitioning from ultra-thick shapes at the root for strength to thinner, high-lift shapes at the tip for speed [2].

II.5.1 The Early Foundations (Aviation Roots)

When the modern wind industry was getting started, engineers didn't reinvent the wheel; they borrowed heavily from classic airplane designs:

NACA Families (4-Digit and 6-Series)

Examples: NACA 4415, NACA 4418, NACA 63-415 (figure II.4)

How they work: Developed by NACA (the predecessor to NASA), these were the first real workhorses of the wind industry. The classic 4-digit series is incredibly forgiving and keeps working well even when dirty. The 6-series focuses on maintaining smooth, laminar flow to cut down on drag [11].

Where you'll find them: Mostly on older or smaller turbines today. Major commercial manufacturers have largely moved away from them because their performance drops significantly when the blades get coated in bugs, dust, or ice.

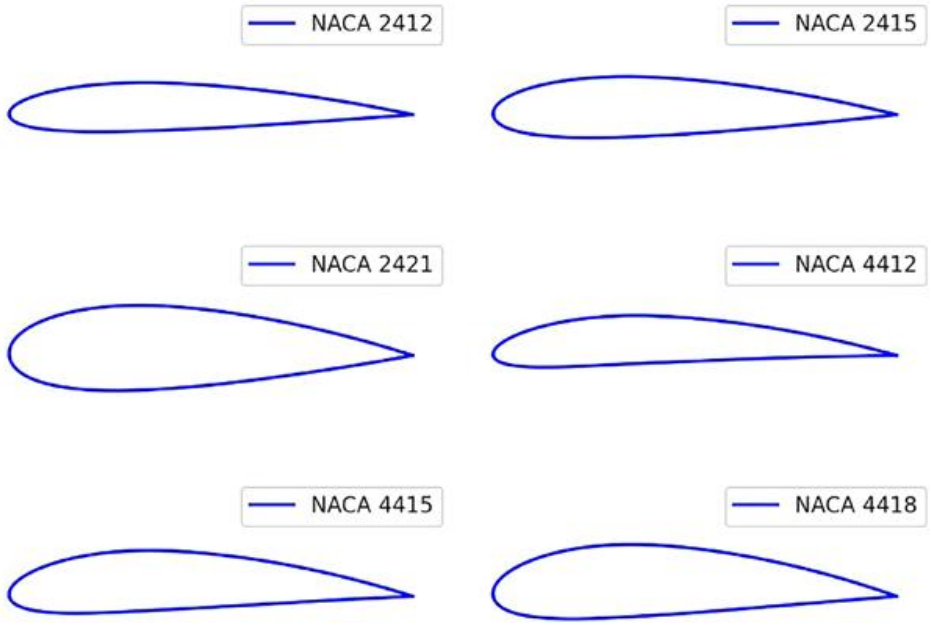


Figure II. 4: Profiles of various NACA 4-digit airfoil families

II.5.2 Dedicated Wind Turbine Families

As turbines grew massive, research labs began engineering airfoils from scratch, specifically tailored for the dirt, turbulence, and structural demands of wind energy:

NREL Families (National Renewable Energy Laboratory, USA)

Examples: S809, S814, S825 (figure II.5)

How they work: Designed specifically for the harsh, unpredictable environments turbines face. Their maximum lift coefficient (C_L) is highly resilient against surface roughness. Crucially, they are designed with a very gentle "stall" profile meaning if the wind angle changes too fast, the blade loses lift gradually rather than snapping, protecting the expensive gearbox and drivetrain from sudden shock loads.

Where you'll find them: Very common in small to medium horizontal-axis wind turbines (HAWTs), with different variations optimized for either the thick or thin parts of the blade.

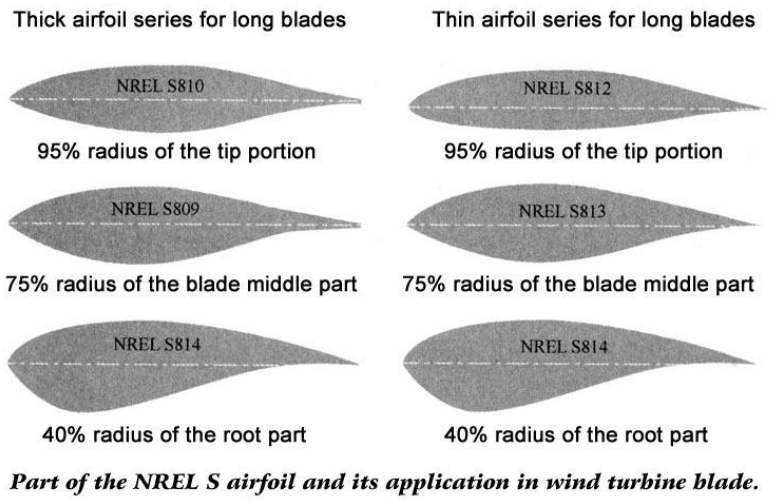


Figure II. 5: NREL S-series airfoils

FFA and Risø Families (Sweden & Denmark)

Examples: FFA-W3, Risø-A1 (figure II.6)

How they work: Created by the Aeronautical Research Institute of Sweden and the Risø National Laboratory in Denmark, these shapes were born to serve the European multi-megawatt boom. They hit the sweet spot of offering high aerodynamic efficiency while remaining physically thick enough to provide structural support for massive blades [12].

Where you'll find them: Heavily utilized in large-scale commercial turbines across Europe, both onshore and offshore.

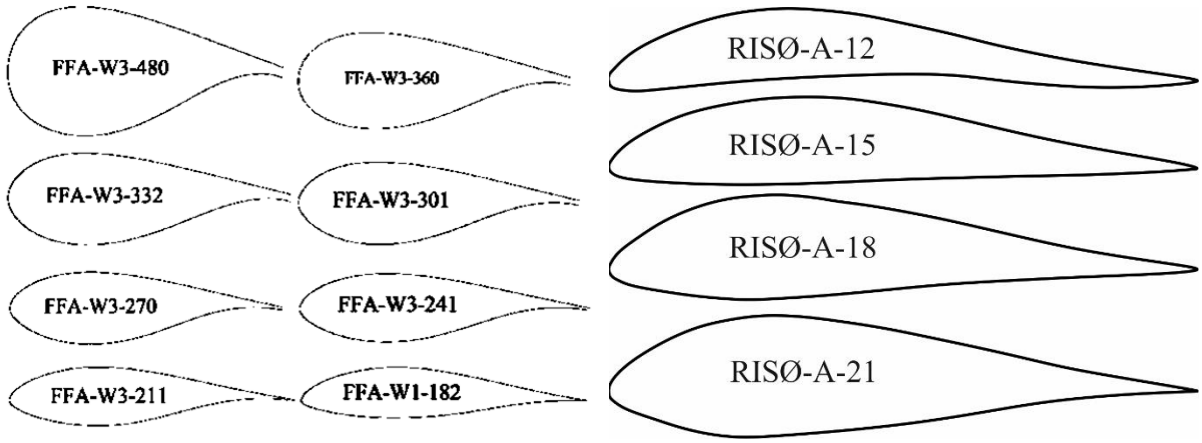


Figure II. 6: Profiles of FFA (left) and RISØ (right)

DU Families (Delft University, Netherlands)

Examples: DU 91-W2-250, DU 97-W-300 (figure II.7)

How they work: Developed at Delft University (the "W" simply stands for wind), these profiles focused on a major engineering headache: making airfoils structurally thick—up to 40% thickness-to-chord ratio—without turning them into massive aerodynamic drags.

Where you'll find them: You'll find these thick profiles near the root and mid-span of massive, modern utility-scale blades where structural strength is just as critical as generating power.

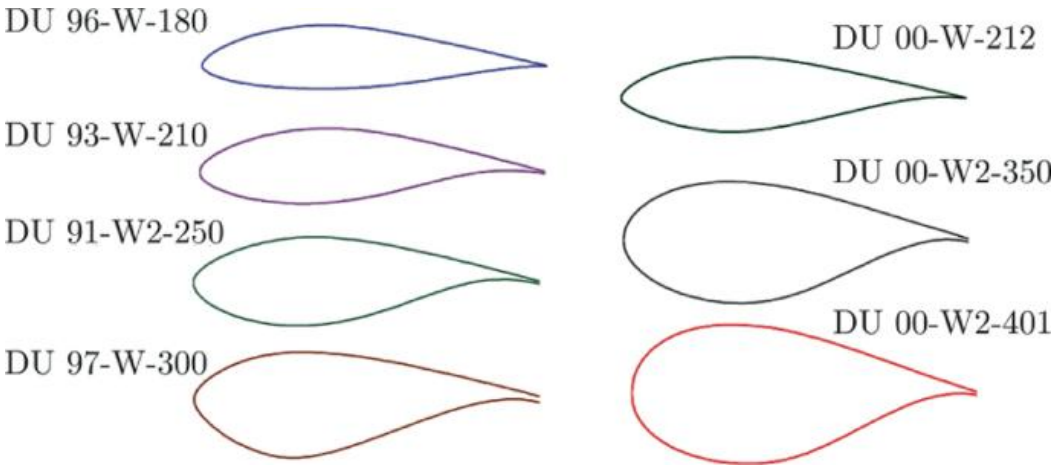


Figure II .7: Profiles of Delft University (DU)

Chapter III

Aerodynamic Modeling and Performance Theories

III.1 Introduction

The primary objective of this chapter is to evaluate and quantify the kinetic energy extracted from the airflow by the wind turbine, as well as to investigate the rotor's geometric design methodology by calculating the optimal distribution of both the twist angle and blade chord length along the span. Furthermore, this chapter covers the application of the Blade Element Momentum (BEM) theory to compute the aerodynamic performance of the turbine, namely the generated power, mechanical torque, and axial thrust force exerted on the rotor. To address this physical problem, the analysis is established based on the Actuator Disk concept, utilizing the Betz Model, which evaluates the dynamic effect of flow velocity reduction across the turbine while neglecting wake rotation behind the rotor.

III.2 Wind Turbine Aerodynamic theories.

The primary function of a wind turbine rotor is to extract the kinetic energy inherent within the oncoming moving air. According to fundamental laws of physics, any fluid mass in motion possesses kinetic energy proportional to its mass flow rate and the square of its velocity. From an aerodynamic perspective, it is physically impossible to extract the entirety of this kinetic energy, as complete extraction would imply a terminal velocity of zero downstream of the rotor, leading to flow stagnation. [13]

To mathematically model this interaction, if the mass flow of air passing directly through the rotor swept area (and thus affected by the turbine's presence) is isolated from the ambient, undisturbed freestream airflow, a distinct boundary surface enclosing the affected fluid mass can be defined. Extending this boundary both far upstream and far downstream establishes a continuous, idealized longitudinal stream tube, as illustrated in figure III.1.

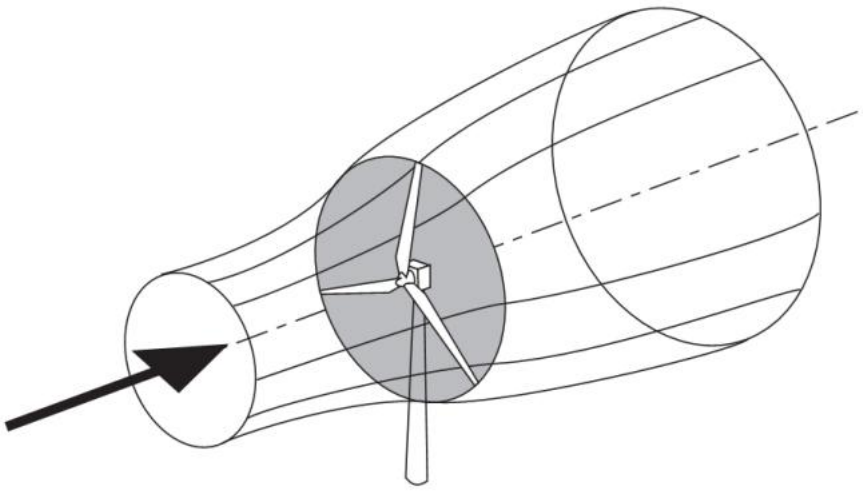


Figure III. 1: Wind energy extraction stream tube

III.2.1 Actuator Disc Theory (Axial Momentum Theory)

The actuator disk model represents the most fundamental analytical framework utilized to evaluate the aerodynamic behavior of wind turbines. Rooted in linear momentum theory (a methodology extensively applied in predicting marine propeller performance) this one-

dimensional approach evaluates a specific control volume as illustrated in figure III.2. This control volume consists of a bounding stream tube and two cross-sections, where the fluid flow is assumed to move continuously across the boundaries. [13]

Within this theoretical framework, the physical wind turbine rotor is idealized as a stationary circular disk positioned at the core of the stream tube. This idealized abstraction is primarily utilized to assess macro-level aerodynamic conversion efficiencies, making the analysis universally applicable regardless of the specific turbine architecture. To maintain mathematical tractability, the model relies on the following governing aerodynamic assumptions:

- A homogeneous, incompressible, and steady-state fluid flow.
- Negligible frictional drag forces.
- An infinite number of rotor blades (infinite solidity approach).
- Uniform axial thrust distribution over the entire disk area.
- A completely non-rotating wake directly behind the rotor.

The static pressure far upstream and far downstream of the rotor equals the undisturbed ambient static pressure.

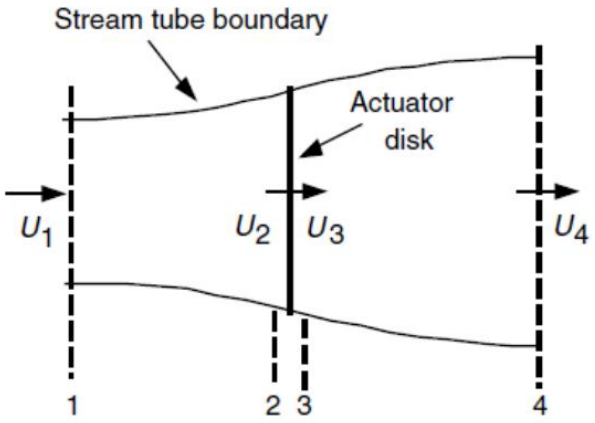


Figure III. 2: Actuator disc stream-tube

Since the total fluid energy differs between the upstream and downstream regions, Bernoulli's equation is applied to derive the governing aerodynamic equations across the rotor. Bernoulli's principle states that the total mechanical energy in a steady, streamline flow (comprising kinetic energy, static pressure energy, and gravitational potential energy) remains constant along any streamline, provided that no net mechanical work is done by or on the fluid within that section, and frictional losses are neglected.

To evaluate the pressure forces acting on the rotor, Bernoulli's equation is applied independently to the flow regions upstream and downstream of the actuator disk, neglecting frictional losses. For the upstream section of the stream tube, extending from the undisturbed far-field (Section 1) to the front face of the disk (Section 2), the energy balance is defined as follows:

$$P_1 + \frac{1}{2}\rho U_1^2 = P_2 + \frac{1}{2}\rho U_2^2 \qquad (III.1)$$

Similarly, applying the principle to the downstream section, from the rear face of the disk (Section 3) to the far wake exit (Section 4), yields:

$$P_3 + \frac{1}{2}\rho U_3^2 = P_4 + \frac{1}{2}\rho U_4^2 \qquad (III.2)$$

Furthermore, by applying the conservation of linear momentum to the designated control volume, the net aerodynamic force exerted on the turbine can be determined. This induced force is equal in magnitude and opposite in direction to the axial thrust force (T). Since the thrust is equivalent to the rate of change of momentum of the air stream across the system, it is formulated as:

$$T = \dot{m}(U_1 - U_4) = \rho U A(U_1 - U_4) \qquad (III.3)$$

Assuming that the far-field static pressures equalize to atmospheric ambient conditions ($P_1 = P_4$), and that the localized velocity remains constant during the disk transition due to continuity ($U_2 = U_3 = U$), the thrust can also be expressed as the net sum of pressure forces acting on each side of the actuator disk area:

$$T = A_2(P_2 - P_3) \qquad (III.4)$$

By subtracting the two equations and applying the baseline assumptions, the final expression for the net pressure drops across the front and back of the rotor is established as:

$$P_2 - P_3 = \frac{1}{2}\rho(U_1^2 - U_4^2) \qquad (III.5)$$

The presence of the actuator disk induces a velocity deficit within the stream tube, which is quantitatively represented by the axial induction factor (a). This dimensionless parameter is defined as the fractional decrease in wind velocity between the undisturbed free-stream flow and the rotor plane. It is mathematically expressed as:

$$a = \frac{U_1 - U_2}{U_1} \qquad (III.6)$$

Consequently, the localized fluid velocity directly at the turbine plane (U_2) can be formulated as a function of the free-stream velocity and the axial induction factor as follows:

$$U_2 = U_1(1 - a) \qquad (III.7)$$

The velocity distribution and fluid pressure profile through the wind turbine system, as a function of the oncoming free-stream wind velocity, are illustrated in figure III.3. This graphical representation explicitly details the fluid dynamic behavior, capturing how the wind velocity experiences a gradual, continuous deceleration as it approaches the upstream face of the rotor, transitions to the localized velocity U_2 directly at the turbine plane, and further diminishes until it stabilizes at its terminal wake velocity U_4 far downstream.

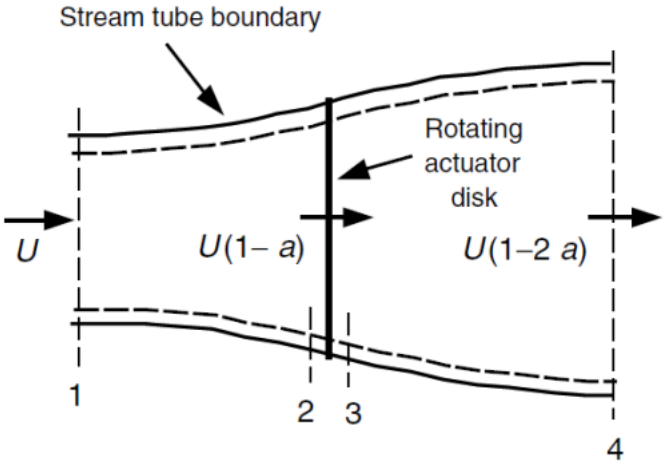


Figure III. 3: Velocity distribution through a wind turbine

The local fluid velocity field across the system comprises two primary components: the undisturbed free-stream velocity and the aerodynamically induced velocity deficit. An increment in the axial induction factor (a) directly yields a significant deceleration of the airflow within the downstream wake region. As the induction factor reaches its theoretical upper limit of a = 0.5, the terminal wind velocity far downstream of the disk drops to zero ($U_4 = 0$).

From a fluid dynamics perspective, a zero-velocity state implies flow stagnation, which acts as a solid aerodynamic blockage that disrupts mass continuity. Therefore, for the mathematical framework of the Actuator Disk Theory to remain valid, the velocity within the far wake must strictly be maintained above zero ($U_4 > 0$) to sustain continuous mass flow rate propagation through the bounding stream tube.

Figure III.4 illustrates both the power coefficient (C_p) of an idealized wind turbine and the non-dimensional downstream wake velocity profile as a function of the axial induction factor (a). The graph demonstrates that the maximum aerodynamic efficiency of an ideal rotor is capped at approximately **59.3%**, universally recognized as the **Betz Limit**. This theoretical derivation emphasizes that maximum energy extraction is strictly achieved when the optimum axial induction factor operates at exactly a = 1/3.

However, in practical engineering applications, the maximum conversion efficiency of even a highly optimized real-world wind turbine remains significantly below this upper Betz limit. Conversely, regarding mechanical loading, experimental and operational thrust coefficients (C_t) can frequently exceed the ideal maximum threshold due to highly turbulent flow states. This performance penalty and subsequent efficiency degradation are driven by several physical phenomena omitted by the baseline actuator disk theory. These critical factors primarily include the parasitic aerodynamic drag (both viscous and induced drag) generated by the blade profiles, alongside high-energy vortex tip and root losses (Tip and Root Losses).

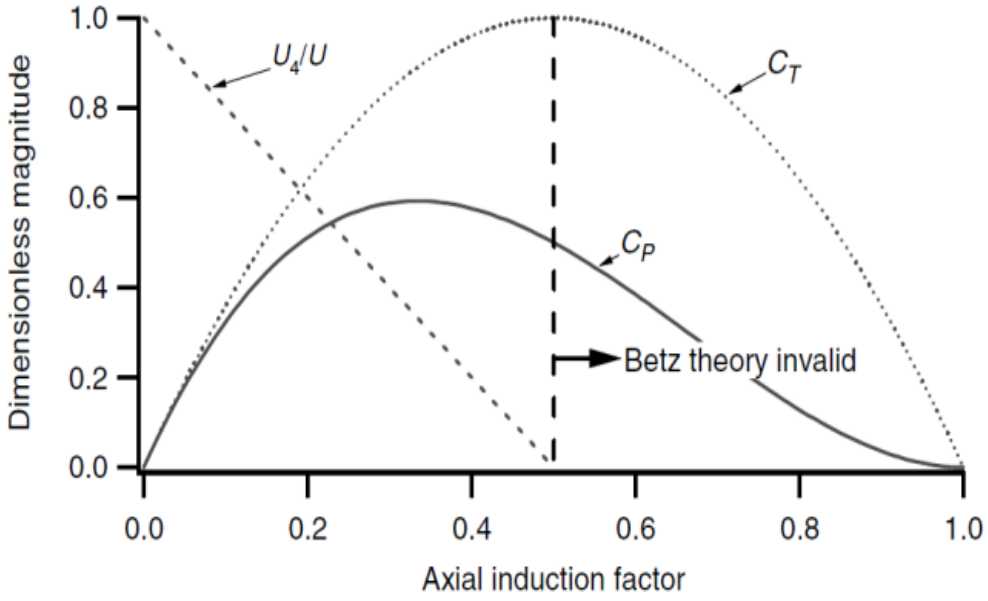


Figure III. 4: The variation in C_P and C_T with axial induction factor

III.2.2 Blade Element Theory (BET)

The Blade Element Theory (BET) is an analytical method employed to predict the aerodynamic forces acting on a wind turbine blade by evaluating the lift and drag forces generated along its span. Within this theoretical framework, the continuous blade structure is discretized into a finite number of independent span-wise elements. Each individual section is assumed to operate aerodynamically decoupled from adjacent elements, behaving effectively as a two-dimensional (2D) airfoil under localized flow conditions. [3]

By utilizing these localized aerodynamic conditions, the lift and drag forces are calculated for each discrete airfoil section. The cumulative sum of these elemental forces is then integrated along the blade length to determine the net mechanical forces and rotational moments exerted on the wind turbine rotor. The mathematical tractability of this theory relies on several governing assumptions: primarily, that there is no aerodynamic cross-talk or interaction between adjacent blade elements, thereby strictly omitting any span-wise radial flow (No Radial Flow). Additionally, it is assumed that the forces acting on the blade are exclusively dictated by the two-dimensional lift and drag coefficients (C_L and C_D) inherent to the selected airfoil geometry. The geometric discretization of the wind turbine blade into a series of distinct elements is schematically illustrated in figure III.5.

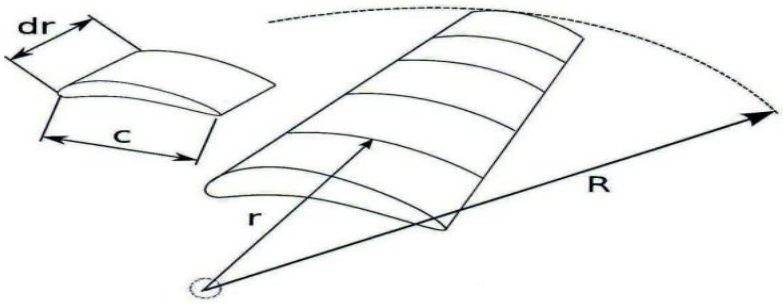


Figure III. 5: Wind turbine blade divided into a series number of sections

In order to determine the local relative wind velocity (V_{rel}) acting on a specific blade section, both the axial and tangential fluid velocity components must be vectorially combined. The resulting velocity magnitude and direction are subsequently utilized to compute the localized lift and drag forces developed at each discrete blade element.

Characterized by the aerodynamic velocity triangle schematically detailed in figure III.6, a discrete section of a wind turbine rotor featuring a blade count of (N), a rotor tip radius of (R), and a local chord length of (c) is evaluated. Assuming the rotor operates at a constant angular velocity of omega under an oncoming free-stream wind velocity, the flow angle is defined as the relative fluid inflow angle subtended between the resultant relative wind velocity vector and the rotor's plane of rotation.

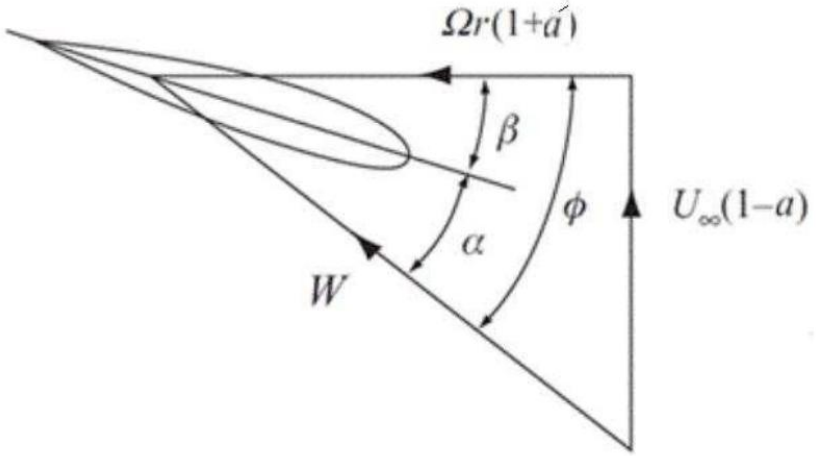


Figure III. 6: Velocities on blade element

Based on the velocity triangle displayed in figure III.6, the local fluid velocity vectors acting upon the blade element are mathematically defined as follows:

- **The Axial Velocity Component (U_A):** This represents the fluid velocity perpendicular to the rotor's plane of rotation, integrated with the axial velocity deficit via the axial induction factor:

$$U_A = U_\infty(1-a) \qquad (III.8)$$

- **-The Tangential Velocity Component (U_T):** This represents the linear velocity driven by the blade's angular rotation at a local radius (r), accounting for the angular momentum imparted to the wake via the tangential (or angular) induction factor (a'):

$$U_T = \Omega r(1+a') \qquad (III.9)$$

By vectorially combining these two orthogonal velocity components using the Pythagorean theorem, the net resultant relative wind velocity (W) striking the airfoil profile is derived as follows:

$$W = \sqrt{U_A^2 + U_T^2} = \sqrt{\left[U_\infty(1-a)\right]^2 + \left[\Omega r(1+a')\right]^2} \qquad (III.10)$$

This resultant relative velocity (W) serves as the fundamental dynamic input required to quantify the elemental lift and drag forces sustained by each discrete blade section.

III.2.3 Blade Element Momentum (BEM) Theory

The Blade Element Momentum (BEM) theory represents the comprehensive mathematical unification of the blade element framework and the classical momentum theory. This integrated approach establishes the foundation for a robust numerical iterative algorithm tasked with predicting localized aerodynamic induction factors and the resulting aerodynamic forces sustained by a wind turbine rotor. [2]

Although the BEM framework is universally implemented across modern wind turbine simulation codes, it relies on specific fluid dynamic simplifications to maintain computational tractability. Crucially, the model assumes a state of quasi-static aerodynamic equilibrium for the airflow circulating around each individual airfoil section. Furthermore, it is postulated that the flow field accelerates instantaneously to adjust to any transient vorticity alterations propagated within the downstream wake region. To establish the mathematical coupling within the BEM framework, the differential thrust and torque acting on a blade element are first derived by resolving the localized lift and drag forces relative to the fluid inflow angle. For a rotor featuring (B) number of blades, these elemental aerodynamic forces are formulated as:

$$dT = \frac{1}{2}\rho W^2 Bc(C_l \cos\phi + C_d \sin\phi)dr \qquad (III.11)$$

$$dQ = \frac{1}{2}\rho W^2 Bc(C_l \sin\phi - C_d \cos\phi)rdr \qquad (III.12)$$

Concurrently, by evaluating the axial thrust as the rate of change of linear momentum through a discrete fluid annulus at radius (r) and width, while incorporating Prandtl's tip loss factor (F) to account for tip vortex penalties, the momentum-based thrust is expressed as:

$$dT = 4\pi\rho r U_\infty^2 a(1-a)Fdr \qquad (III.13)$$

Similarly, the differential aerodynamic torque is equated to the rate of change of angular momentum within the expanding wake, integrated with the tip loss correction factor (F):

$$dQ = 4\pi\rho r^3 U_\infty \Omega a'(1-a)Fdr \qquad (III.14)$$

In order to determine the definitive values of both the axial (a) and tangential (a') induction factors, a numerical iterative algorithm must be implemented. By equating the blade element forces to the momentum conservation equations, and introducing the localized rotor solidity parameter, the final governing equations utilized to compute and update the induction factors per iteration are derived as follows:

$$\frac{a}{1-a} = \frac{\sigma(C_l \cos\phi + C_d \sin\phi)}{4F\sin^2\phi} \qquad (III.15)$$

$$\frac{a'}{1+a'} = \frac{\sigma(C_l \sin\phi - C_d \cos\phi)}{4F\sin\phi\cos\phi} \qquad (III.16)$$

These decoupled formulations are solved implicitly through successive iterations until numerical convergence criteria for the induced flow velocities are satisfied.

The blade solidity is defined as the ratio of the total physical blade area to the swept area of the rotor disk. At any local radial position (r), this dimensionless aerodynamic parameter is expressed as:

$$\sigma = \frac{B \cdot c}{2\pi r} \qquad (III.17)$$

It is computationally critical to note that the Blade Element Momentum (BEM) theory remains valid only under the assumption of uniform flow circulation along the blade span, which implies a uniform axial induction factor (a). In scenarios characterized by non-uniform circulation, radial interactions and momentum exchanges inevitably occur between the fluid

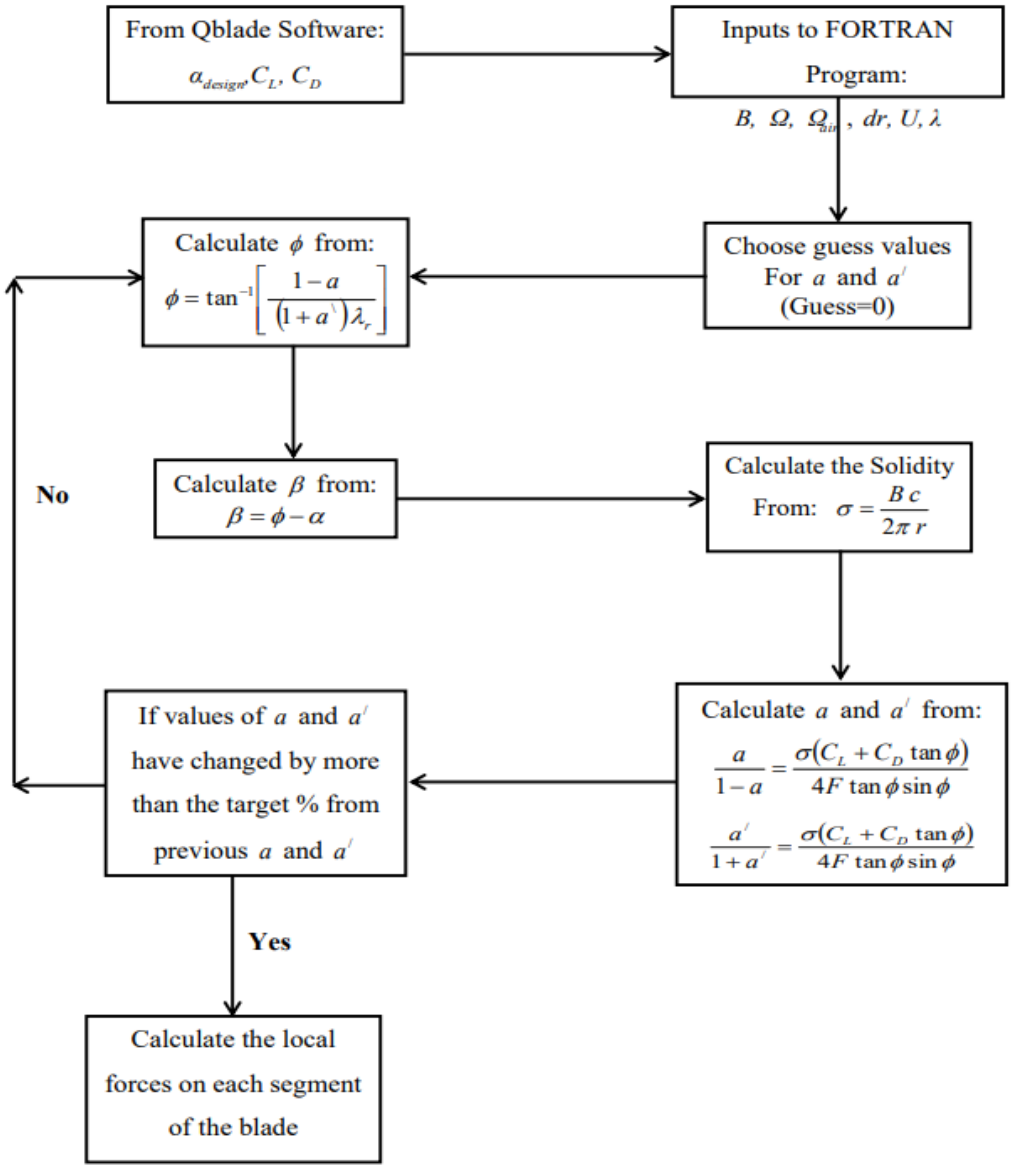


Figure III. 7: Flow chart of BEM theory

streams propagating through adjacent elemental annular rings, violating the foundational BEM assumption of mutually independent blade elements (figure III.7).

Chapter IV

PARAMETRIC STUDY OF A SMALL WIND TURBINE USING QBLADE SOFTWARE

IV.1. Introduction

Given the rapid development in the renewable energy sector, technical requirements aimed at improving aerodynamic efficiency, maximizing energy production, and extending the operational lifespan of wind turbines have increased. These turbines play a pivotal role in extracting wind energy and converting it into electrical energy. In this regard, researchers focus on studying mechanical stresses and aerodynamic phenomena to deeply understand the complex behavior of blades and enhance their performance. To achieve an accurate simulation that mimics real operating conditions, the **QBlade** software is considered one of the most prominent globally approved tools in this field. The software bases its computations on the Blade Element Momentum (**BEM**) theory and features an integrated library of aerodynamic profiles (airfoils). Based on these engineering features, QBlade represents a high-precision and reliable simulation tool for analyzing and designing wind turbine blades.

IV.2. Definition of QBlade

QBlade is an advanced, open-source wind turbine calculation and design software. It provides an integrated framework for the aerodynamic design, structural modeling, and aeroelastic simulation of both Horizontal Axis Wind Turbines (HAWT) and Vertical Axis Wind Turbines (VAWT) (figure IV.1). [13]



Figure IV. 1: The Main Interface of QBlade Software

IV.3. Functionalities of QBlade

The QBlade software incorporates a comprehensive range of functionalities, including:

- **360° Polar Extrapolation:** Extrapolating XFOIL generated or imported polar data over a full 360° angle of attack range.
- **Blade Design and Optimization:** Designing and optimizing aerodynamic blades, including 3D rotor geometry, utilizing generated or imported XFOIL airfoils.
- **Wind Turbine Definition:** Defining full turbine configurations and operational modes (rotor dynamics, control strategies, generator types, etc.).

- **Rotor Performance Evaluation:** Computing rotor aerodynamic performance as a function of the Tip Speed Ratio (TSR).
- **Multi-Parametric Rotor Simulation:** Simulating rotor behavior and characteristics under various multi-parameter configurations.
- **Turbine Efficiency Assessment:** Calculating wind turbine power curves and efficiency across a comprehensive range of wind speeds.
- **Annual Energy Production (AEP) Estimation:** Computing the expected annual energy yield based on the Weibull wind speed distribution model.
- **Flexible Parameter Access:** Direct access to all internal simulation variables for flexible data manipulation and aeroelastic coupling.
- **Data Post-Processing and Visualization:** Advanced tools for data processing and dynamic graphical rendering of simulation fields.
- **Turbulent Inflow Generation:** Generating turbulent wind inflow fields adhering to the statistical Veers model.
- **Manual Correction Selection:** User-defined selection of aerodynamic correction algorithms for the Blade Element method (e.g., tip and hub loss corrections).
- **Project Database Management:** Structured storage and retrieval of projects, rotors, turbines, and simulation run within an integrated runtime database.

IV.4. Practical steps for conducting a wind turbine study in QBlade

To illustrate the practical steps required for analyzing a wind turbine using QBlade, a case study was conducted using the NACA4412 airfoil to design a rotor with a radius of 0.35 m. This parametric simulation aims to optimize the spanwise distribution of the twist angle and chord length to maximize the aerodynamic efficiency, thereby extracting the ultimate power and energy yield from the turbine. The operational workflow initiates at the airfoil engineering level, where the first step involves importing the coordinate file of the airfoil into the software environment to proceed with design and analysis (figure IV.2).

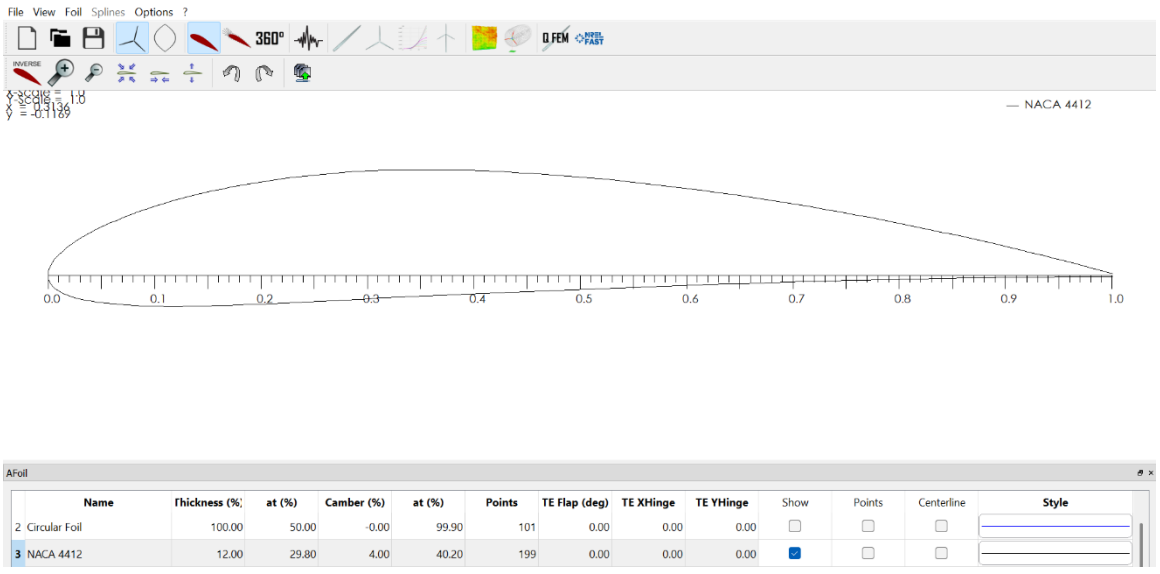


Figure IV. 2: Coordinates of the imported NACA4412 airfoil

These results present the aerodynamic analysis of the NACA4412 airfoil, displaying both the lift coefficient (C_L) and the drag coefficient (C_D) as a function of the angle of attack. The primary significance of these polar curves lies in identifying the optimum angle of attack, which yields the maximum aerodynamic efficiency ratio (C_L/C_D) for the airfoil, ensuring optimal kinetic energy extraction from the wind (figure IV.3).

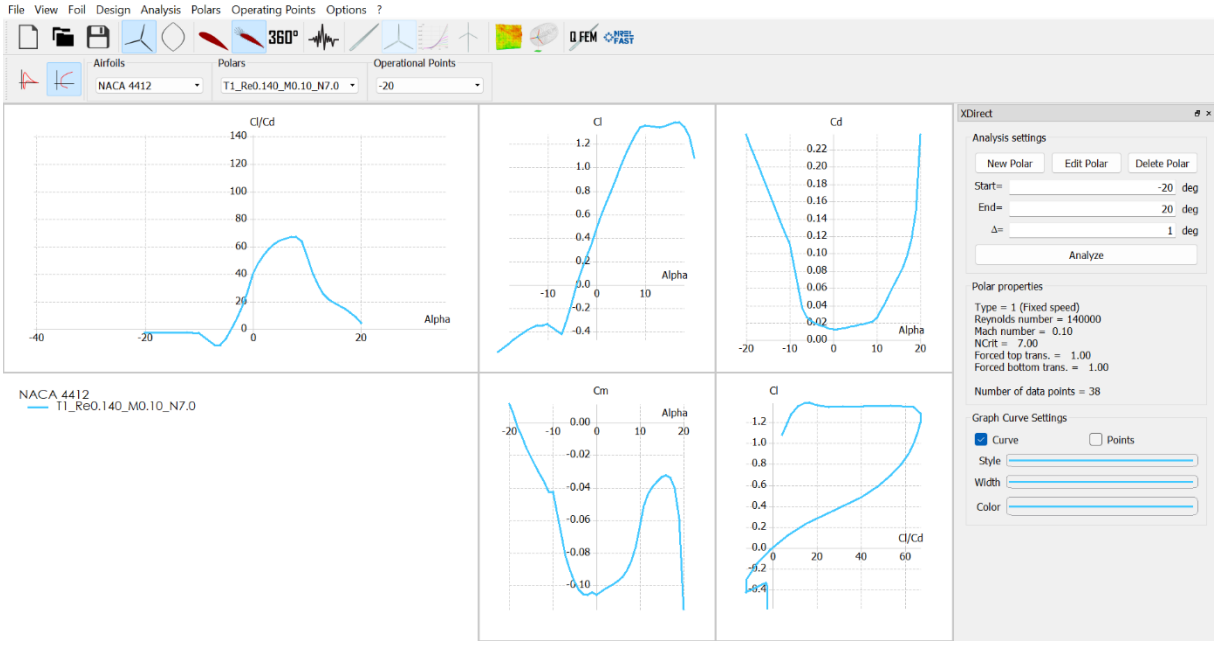


Figure IV. 3: Distribution of Lift and Drag Coefficients and the Lift-to-Drag Ratio

This figure illustrates the pressure distribution over the studied NACA4412 airfoil, clearly demonstrating the variance in aerodynamic force distribution over the blade's upper and lower surfaces between the two configurations. This discrepancy is directly attributed to the change in the angle of attack, which fundamentally governs the surrounding pressure field. Furthermore, the curves depict the variation of the pressure coefficient (C_p) along the chord length, which is heavily influenced by the angle of attack, thereby explaining the generation of lift due to the pressure differential between the suction and pressure sides (figure IV.4).

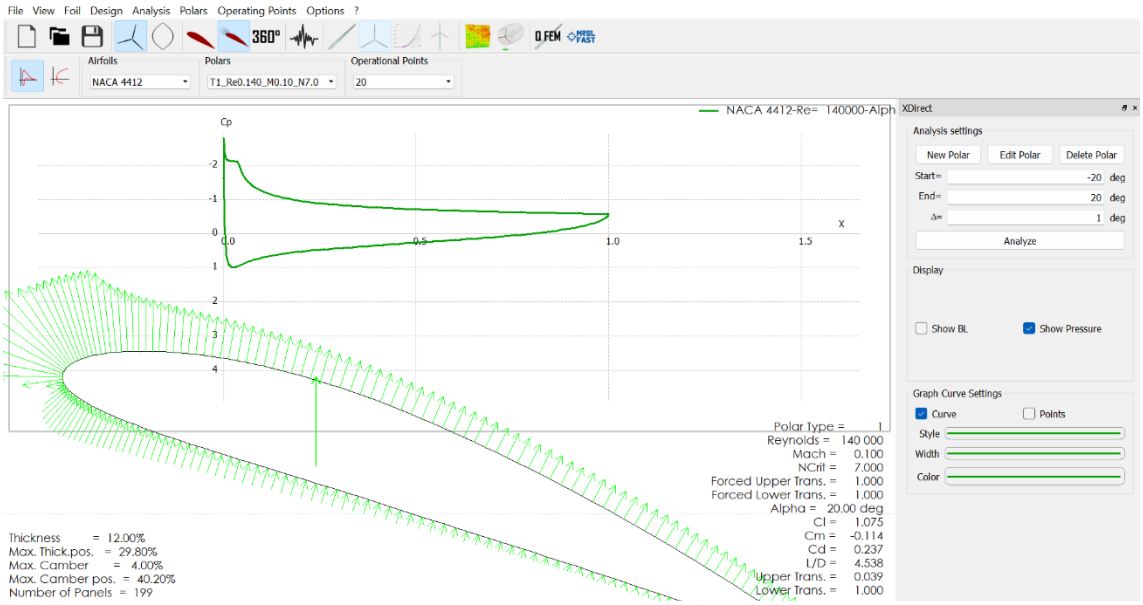


Figure IV. 4: Power Coefficient Curve and Pressure Distribution

This curve illustrates the variations of the lift coefficient (C_L), drag coefficient (C_D), and the lift-to-drag ratio (C_L/C_D), integrated into the 360° extrapolated polar curve. Furthermore, the results indicate that these coefficients remain constant for the circular (cylinder) profile regardless of the angle of attack, in contrast to the aerodynamic behavior of the NACA4412 airfoil, which is highly sensitive to flow orientation (figure IV.5).

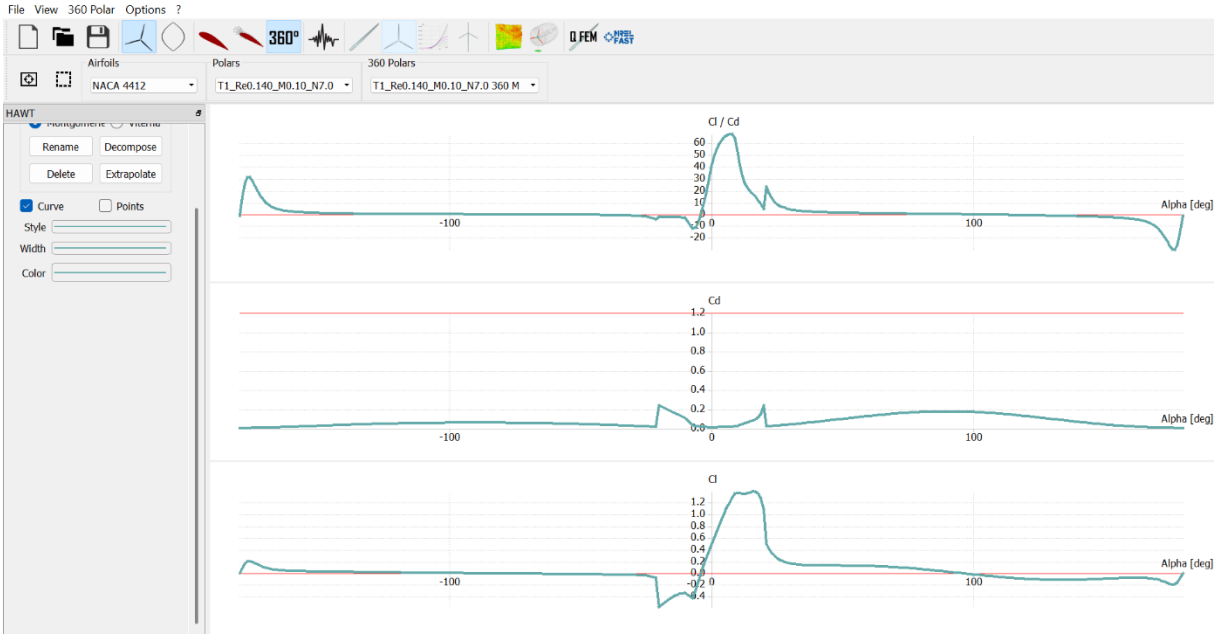


Figure IV. 5: 360° Polar Extrapolation Module

At this stage, the process transitions to the aerodynamic blade design using the NACA4412 airfoil. This module allows precise control over the chord length distribution, twist angle, and radial position of each station along the blade span. By integrating these two-dimensional (2D) profiles, the three-dimensional (3D) rotor blade geometry is generated. Furthermore, the configuration allows full control over the total blade count of the rotor according to the design specifications (figure IV.6).

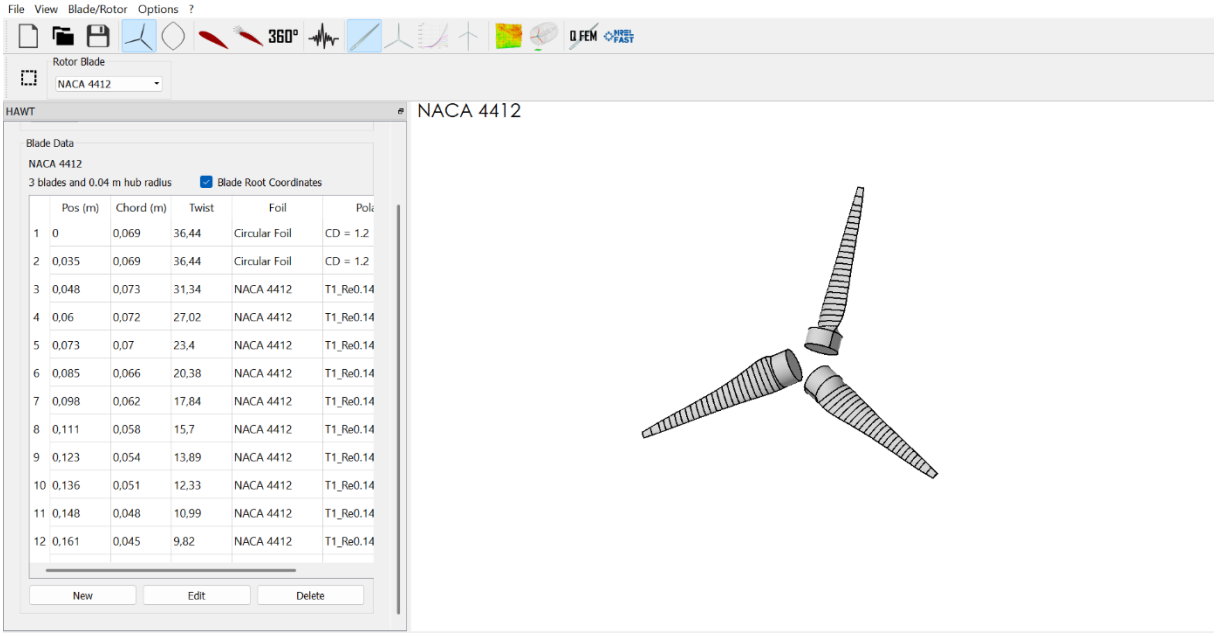


Figure IV. 6: Design Module

In this section, the Blade Element Momentum (BEM) theory is utilized to compute the aerodynamic parameters and performance characteristics of the rotor. This stage enables the evaluation of how variations in the Tip Speed Ratio (TSR) influence key performance coefficients (such as the power coefficient C_p and torque coefficient C_m). Additionally, it allows for a comparative analysis to investigate the impact of the blade count on the extracted power as a function of the tip speed ratio or the rotor's rotational speed (figure IV.7).

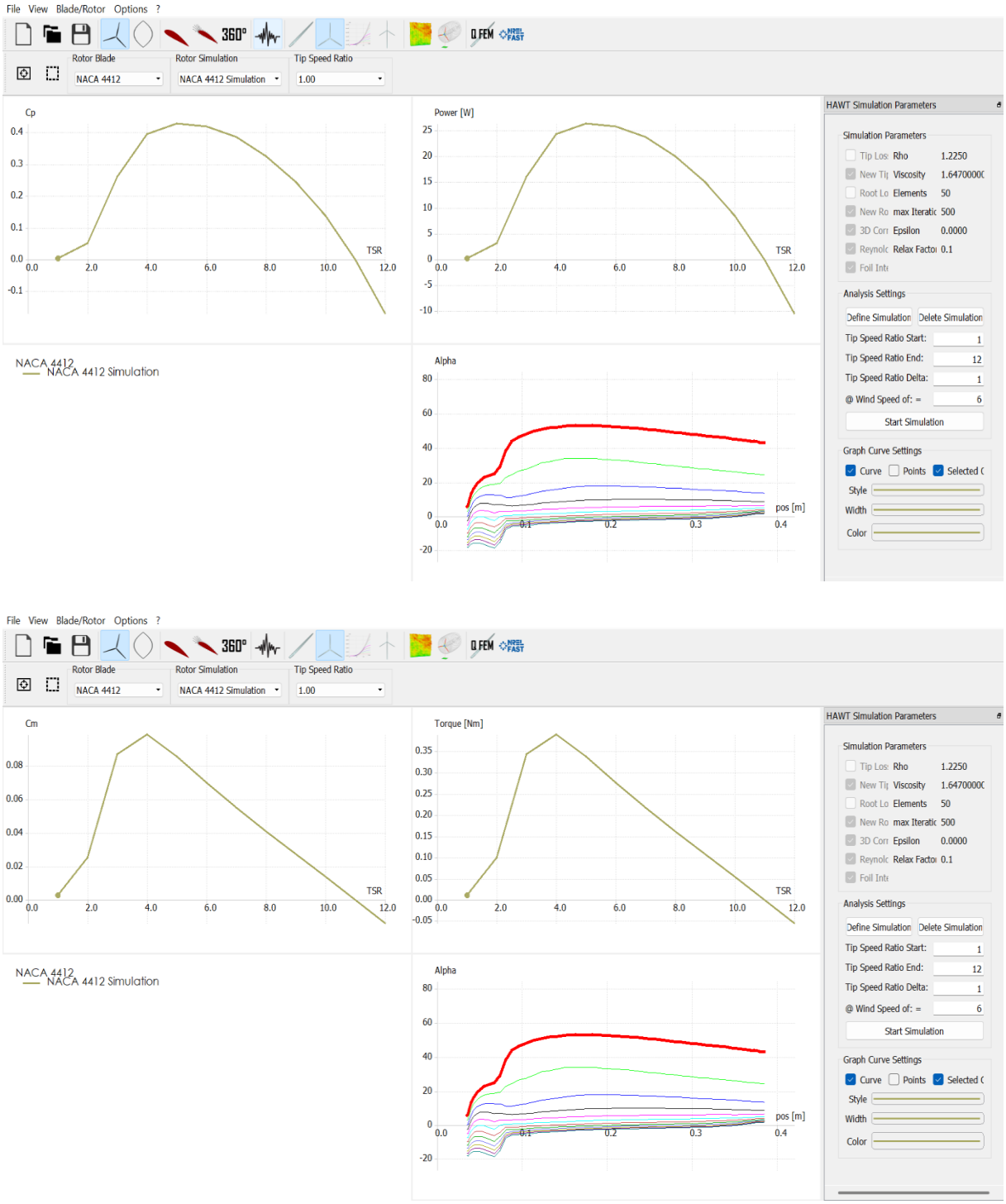


Figure IV. 7: Rotor Simulation using Blade Element Momentum (BEM) Theory

In this section, all aerodynamic coefficients and variables computed via the BEM theory are analyzed. This step allows for the precise evaluation and control of all parameters governing the dynamic performance of the turbine blades. Consequently, it enables the prediction of the extracted power as a function of various operational and environmental factors, primarily the free-stream wind speed and the Tip Speed Ratio (TSR) (figure IV.8).

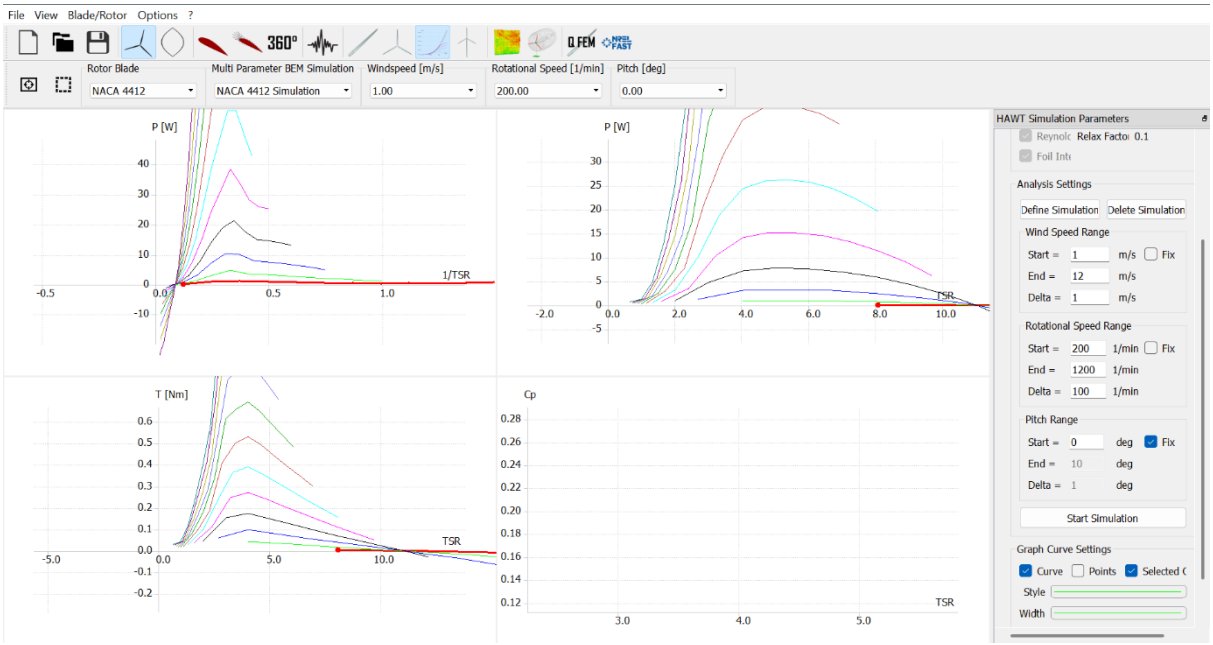


Figure IV. 8: Multi-Parameter Simulation Module

This three-dimensional plot illustrates the non-linear distribution of the lift force generated along the blades within the rotational domain. This distribution exhibits an unsteady (time-dependent) behavior, providing a highly accurate and comprehensive insight into the aerodynamic lift generation mechanisms of the turbine, based exclusively on the fundamentals of potential flow theory (figure IV.9).

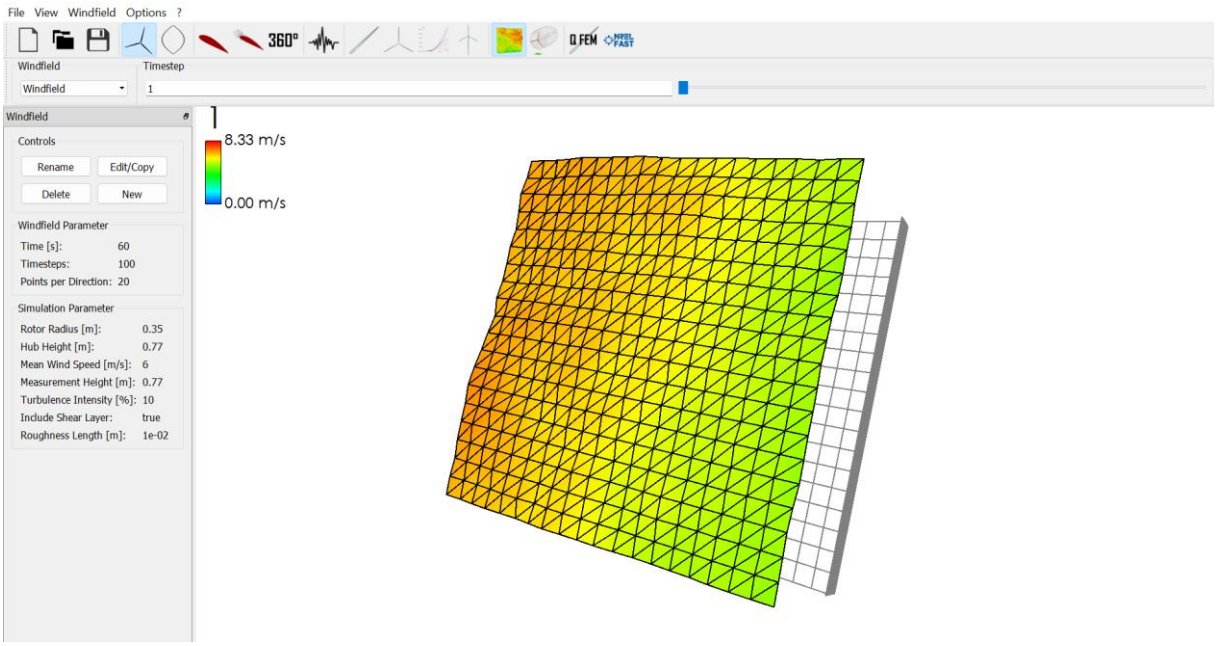


Figure IV. 9: Turbulent Windfield Generator Module

During the rotation of the turbine blade, the streamlines striking the leading-edge split into two paths: an upper path characterized by converging streamlines (higher velocity and lower pressure), and a lower path characterized by diverging streamlines (lower velocity and higher pressure). Upon reaching the trailing edge, these streams rejoin, generating turbulent wake vortices. In addition to these vortices, tip and root vortices form at the blade's structural boundaries with a higher intensity due to the presence of free ends. The pressure differential causes the air to migrate from the high-pressure lower surface to the low-pressure upper surface around the tips, creating trailing vortex filaments. The induced velocity field generated by these vortices can be computed using the Biot-Savart law, while the lift force can be evaluated using the Kutta-Joukowski theorem, which establishes a fundamental relationship between lift, induced velocity, and fluid circulation (figure IV.10).

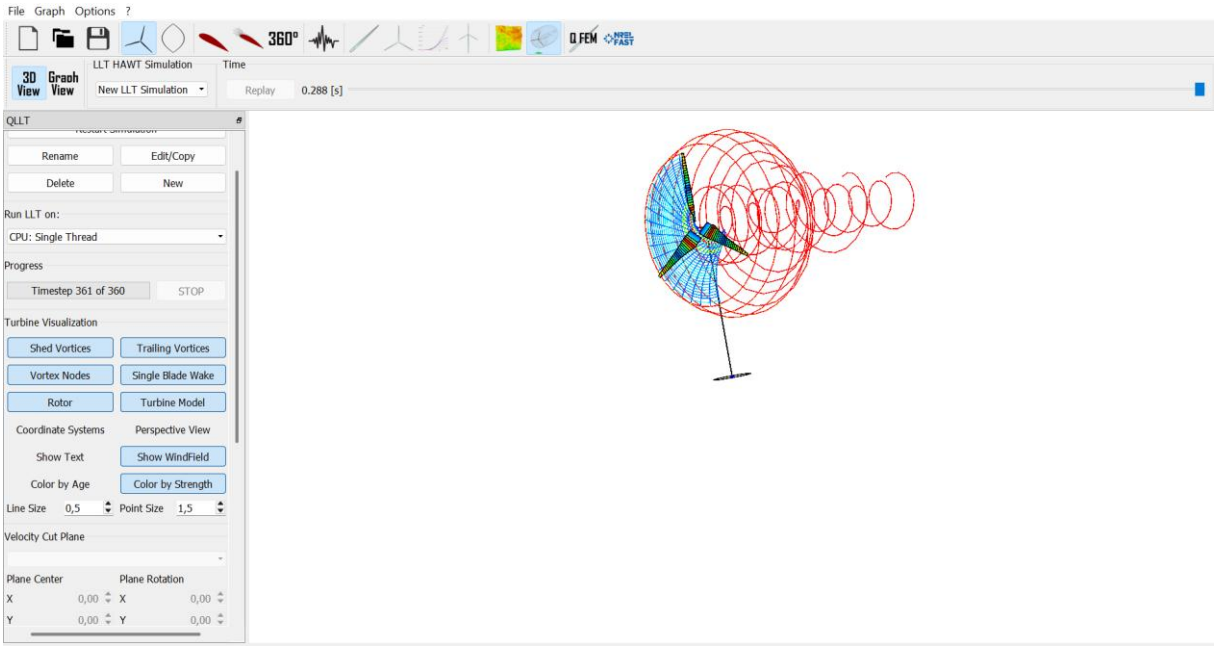


Figure IV. 10: Free Wake Vortex Simulation Module

IV.5. Validation of the Numerical Model

In the context of evaluating the results and analyzing the outputs of the numerical simulations performed in this chapter, and to establish a rigorous scientific foundation for the adopted aerodynamic approximations and computational models, an extensive comparative analysis was conducted against established academic benchmarks. Specifically, this validation process relies on the prominent study authored by **Mohamed Khaled Mohamed Mohamed Hasanin (2017)**, titled:

'The Effect of Blade Geometry and Configuration on Horizontal Axis Wind Turbine Performance',

which investigated the impact of blade geometric variations and rotor configurations on the overall dynamic performance of Horizontal Axis Wind Turbines (HAWT).

Crucially, and what highlights the unique merit of our findings, is that the reference study heavily utilized advanced aerodynamic and structural optimization features to achieve the absolute maximum efficiency for its blade designs. Nevertheless, when conducting a parametric graphical comparison between both works, a remarkable and significant convergence in overall behavior and peak efficiency values is observed.

This hydrodynamic convergence is explicitly demonstrated when analyzing the lift-to-drag ratio (C_L/C_D) as a function of the angle of attack for the airfoils. Both curves follow an identical ascending profile towards the optimal glide ratio before entering the aerodynamic stall region. This superior aerodynamic efficiency at the airfoil level directly influenced the full rotor performance, as confirmed by the power coefficient (C_p) vs. Tip Speed Ratio (TSR) curves of both studies. The peak performance values (Peak C_p) exhibit a tight correlation, and the curve trajectories align precisely across different rotational speeds.

This close proximity to an optimized aerodynamic model does not merely validate the mathematical computations; rather, it serves as definitive and compelling evidence of the high efficiency and superior geometric design of our studied turbine. It demonstrates that our parametric selections during the initial design phase (such as aerodynamic airfoil selection and twist angle distribution) were highly effective and mathematically sound. Furthermore, this exceptional convergence reflects the outstanding competence and rigor of the simulation study we conducted, proving that our turbine configuration achieves a high-tier dynamic performance that rivals optimized academic models, thereby ensuring top-level academic reliability and engineering viability for this research (figures IV.11 and IV.12).

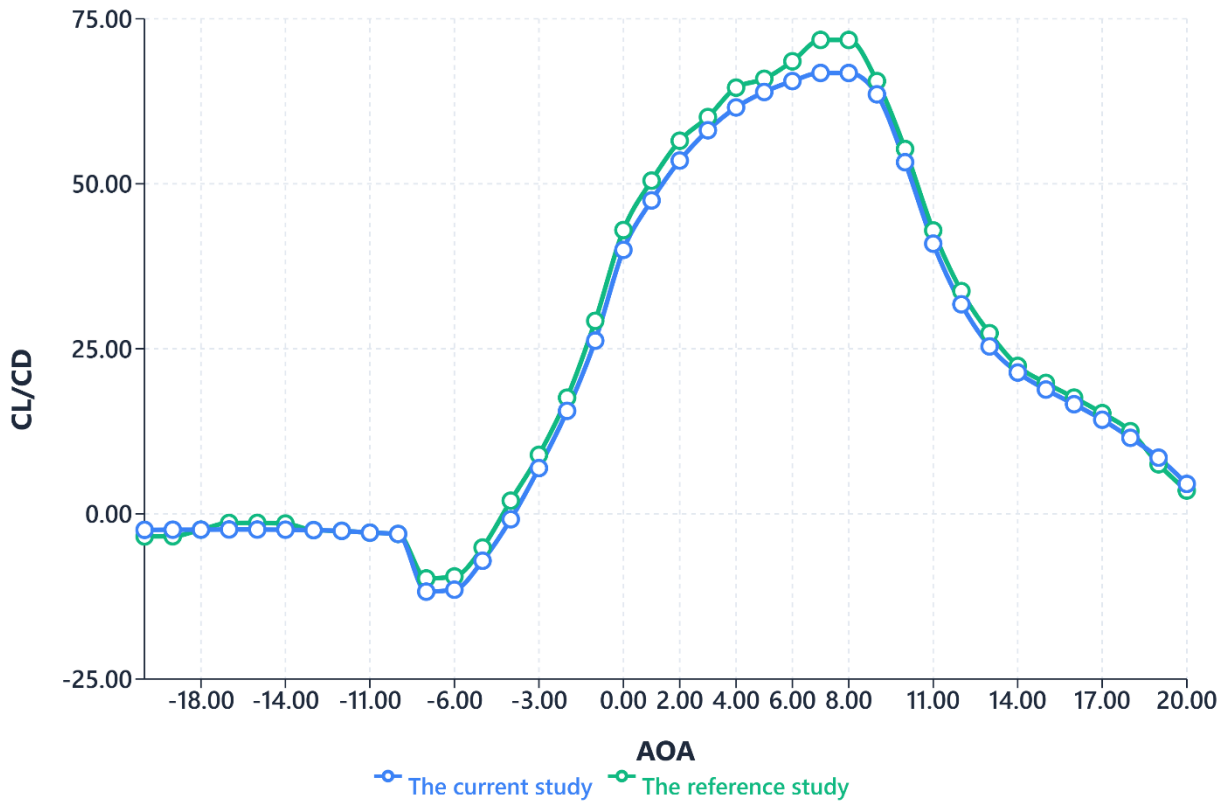


Figure IV. 11: Comparison of the aerodynamic efficiency between the current study and the reference study



Figure IV. 12: Comparison of the power coefficient between the current study and the reference study

IV.6. Aerodynamic Performance Comparison of Candidate Airfoils

Before establishing the final blade configuration, a preliminary aerodynamic optimization study was carried out to evaluate three distinct candidate airfoil profiles: NACA 4412, SG6040, and SG6043. The primary objective was to isolate the profile that delivers the superior lift-to-drag ratio (Lift-to-Drag Ratio), which directly dictates the dimensionless power coefficient (Cp) and overall kinetic extraction efficiency of the rotor (figures IV.13 and IV.14).

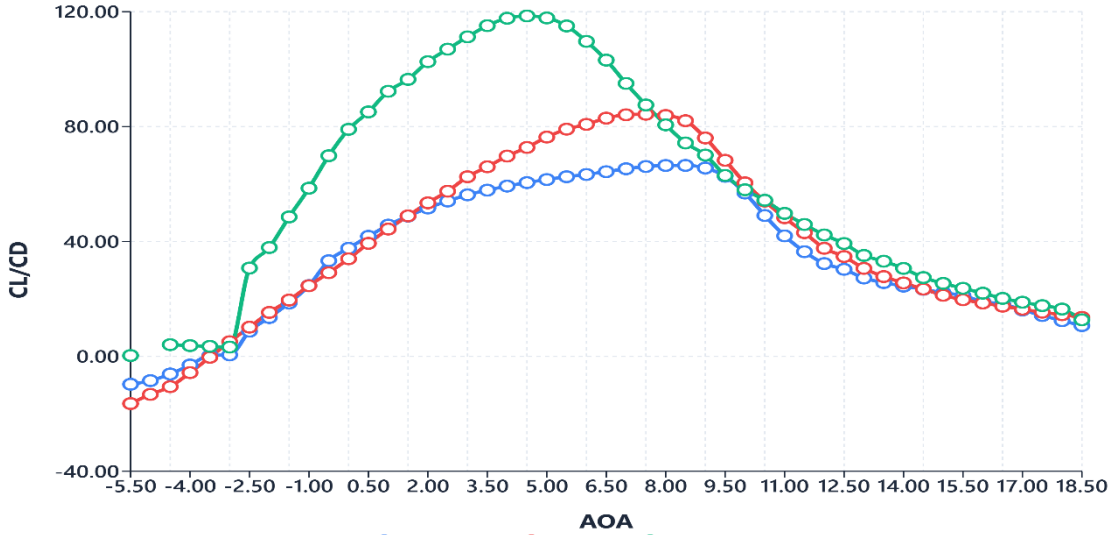


Figure IV. 13: Comparison of aerodynamic efficiency for the selected airfoils (NACA4412, SG6040, SG6043)

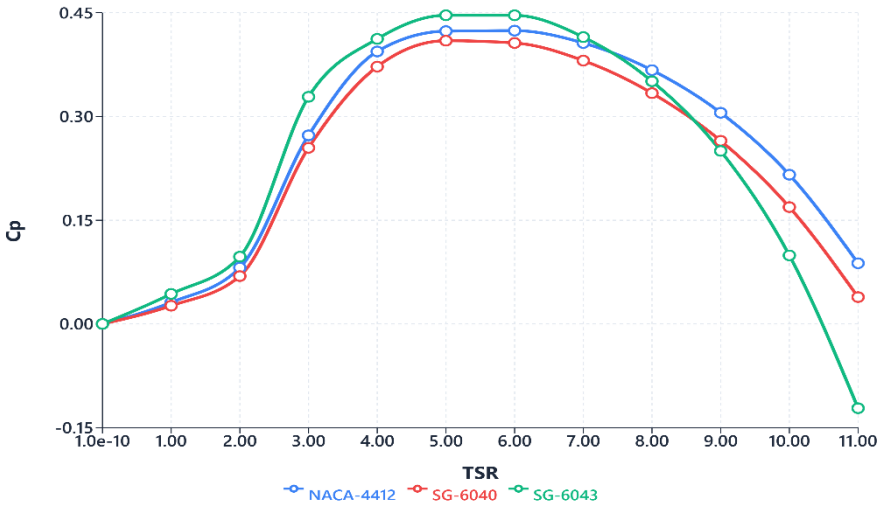


Figure IV. 14: Comparison of power coefficient
for the selected airfoils (NACA4412, SG6040, SG6043)

The numerical simulation results indicated a clear divergence in the aerodynamic behavior of the tested airfoils. The NACA 4412 profile exhibited standard performance with stable lift generation but suffered from a relatively higher drag coefficient at elevated angles of attack. On the other hand, the thicker SG6040 profile demonstrated a high lift capacity at lower speeds, making it aerodynamically robust but penalized by enhanced skin friction and form drag due to its geometric thickness.

Ultimately, the SG6043 airfoil emerged as the most aerodynamically efficient profile among the selected candidates. It achieved the absolute highest lift-to-drag ratio and delivered the maximum power coefficient (Cp) across the operational spectrum. This superior performance is fluid-dynamically attributed to its slender, highly engineered camber line, which successfully suppresses boundary layer separation, minimizes trailing-edge wake losses, and optimizes pressure distribution across the suction and pressure sides of the blade.

IV.7. The Aero-Structural Trade-off and Proposed Hybrid Solution

However, despite the exceptional aerodynamic supremacy and high energy conversion efficiency of the SG6043 profile, a major engineering challenge arises regarding its structural baseline. Due to its ultra-thin geometric nature, a blade fabricated exclusively from the SG6043 profile suffers from severe structural vulnerability, particularly along the inner span where the mechanical loads are maximum. Under real operational conditions, this extreme thinness fails to provide the required area moment of inertia, leaving the blade highly susceptible to massive stress concentrations, critical fatigue, and sudden mechanical fracture at the hub interface.

To resolve this classic aero-structural conflict without sacrificing the rotor's power extraction capability, an optimized hybrid blade design was proposed. This strategy leverages the strengths of multiple geometries by forming a multi-section transition along the blade span:

- **From r = 0 m to r = 0.035 m:** A standard circular foil is used strictly for secure hub mounting and mechanical adaptation.

- **From r = 0.035 m to r = 0.085 m:** The thicker SG6040 airfoil is strategically deployed over this critical 5 cm root span to act as a heavy-duty structural anchor, providing the necessary thickness to absorb intense bending moments.

- **From r = 0.085 m to r = 0.35 m:** The blade transitions smoothly back into the high-performance, slender SG6043 profile to exploit its maximum aerodynamic efficiency along the upper power-producing span.

IV.8. Comparative Structural Integrity and Aerodynamic Loading

To assess the engineering feasibility and validate the mechanical structural integrity of the proposed blade architecture, a detailed comparative simulation was conducted under optimal aerodynamic operating conditions at a Tip Speed Ratio (TSR) of 5.5. This specific operational point corresponds to the peak power coefficient (Cp), where the turbine achieves its maximum kinetic energy extraction while simultaneously facing its most severe aerodynamic thrust forces and mechanical torque loads.

The structural performance evaluation focuses on a direct comparison between two distinct blade configurations, tracking their spatial Von-Mises stress distribution and kinematic tip deflections:

1. **The Baseline Configuration:** Features a standard circular foil section from the rotational center r = 0 m to r = 0.035 m for hub mounting, transitioning immediately into the slender SG6043 airfoil profile across the entire remaining span.

2. **The Optimized Hybrid Configuration:** Incorporates the same circular foil from r = 0 m to r = 0.035 m but introduces the thicker SG6040 airfoil as a localized structural reinforcement over a 5 cm span from r = 0.035 m to r = 0.085 m. Beyond this root transition zone, the blade shifts smoothly into the aerodynamic SG6043 profile up to the free tip (r = 0.35 m).

The comparative performance is systematically analyzed across the following core technical metrics:

a. Aerodynamic Boundary Loading Profiles at the Blade Root

The numerical flow data indicates that the inner span from r = 0.035 m to r = 0.085 m (where the thicker profile is integrated) experiences the most turbulent fluid-structure interactions on the entire rotor:

- **Tangential Forces:** Severe localized flow separation and hub-vortex configurations generate negative braking loads that drop to a sharp peak of -0.0545 N. This behavior induces severe cyclic shear stresses and dynamic twisting moments near the hub interface.

- **Normal Loading:** Simultaneously, the axial thrust forces responsible for out-of-plane bending moments escalate rapidly within this 5 cm transition band, expanding from 0.0421 N to over 0.0582 N.

This combined action of high normal thrust and negative tangential braking isolates the root region as the absolute critical stress zone of the entire assembly (figures IV.15 and IV.16).

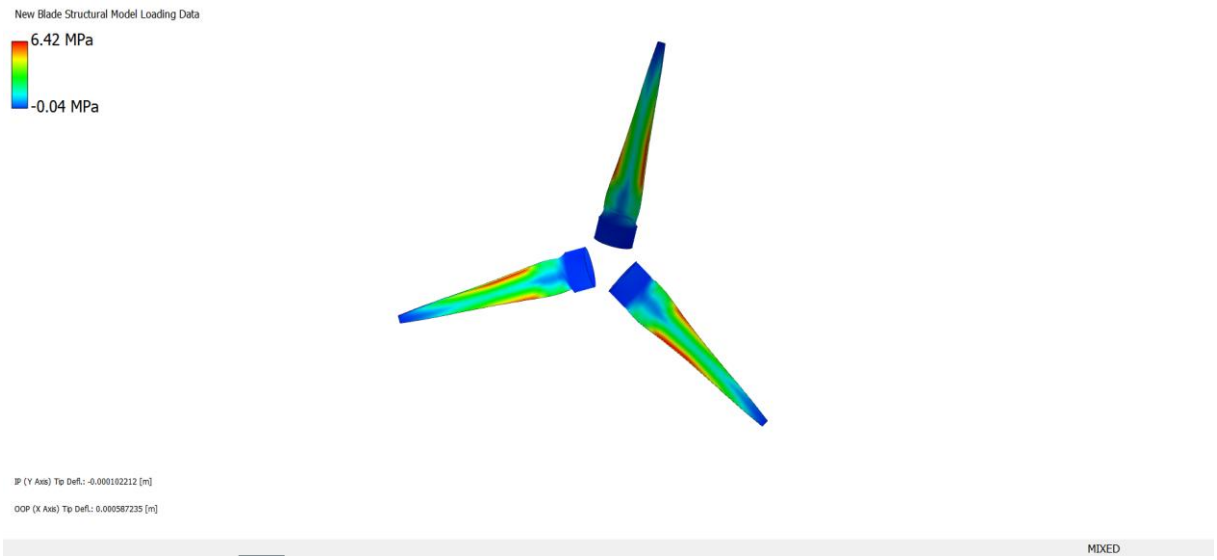


Figure IV. 15: Blade structural model showing stress distribution in mixed blade

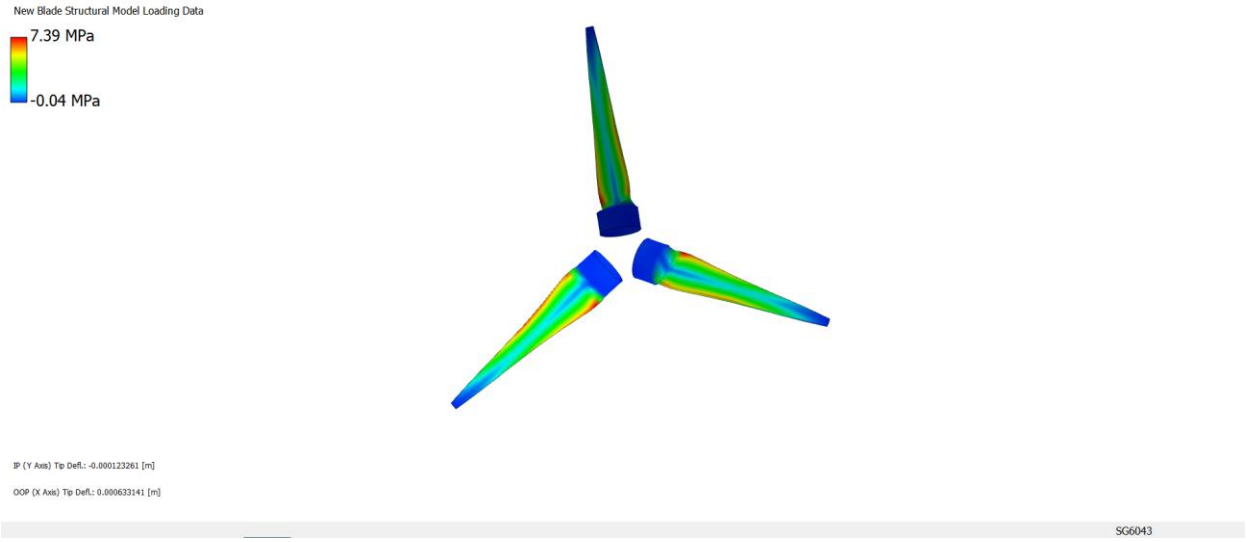


Figure IV. 16: Blade structural model showing stress distribution in SG6043 only

b. Comparative Von-Mises Stress Distribution

The structural response of the blade material to these intense root boundary loads varies significantly depending on the cross-sectional geometry:

- **The Baseline Blade (SG6043):** Utilizing an ultra-thin aerodynamic profile right after the circular adapter leaves the root structurally vulnerable. The slender cross-section lacks the necessary area moment of inertia (I) to handle the heavy bending moments. This geometry forces a dangerous localized stress concentration at the hub interface, driving the peak Von-Mises stress up to a critical 7.39 MPa. Such elevated stress levels severely compromise the structural safety factor, increasing the risks of fatigue failure or sudden material fracture.

- **The Hybrid Blade (Mixed):** Deploying the thicker SG6040 profile across the critical 5 cm root span provides an exceptionally robust mechanical buffer. The increased thickness-to-chord ratio (t/c) raises the sectional rigidity exponentially. Consequently, the maximum Von-Mises stress drops to 6.42 MPa, yielding a highly valuable 13.12% reduction in global material stress. The stress contours demonstrate a highly uniform, smooth gradient where structural loads are safely distributed away from the root into the main blade body.

c. Kinematic Tip Deflection and Displacement Analysis

The structural rigidity gained by optimizing the root geometry (0.035 m to 0.085 m) directly influences the mechanical stability of the distant blade tip (r = 0.35 m):

- **Out-of-Plane Deflection (X -axis):** The hybrid design restricts the axial displacement caused by oncoming wind thrust, lowering it from 0.000633 m in the baseline model to 0.000587 m. This 7.25% increase in structural stiffness ensures a safer clearance margin and effectively eliminates tower-strike risks.

- **In-Plane Deflection (Y -axis):** Thanks to the enhanced resistance against the negative tangential root loads, the rotational deflection along the Y -axis is constrained from -0.000123 m down to -0.000102 m. This represents a 17.07% improvement in rotational balance, maintaining the precise aerodynamic pitch angle during high-speed operation.

d. Aero-Structural Optimization Synthesis

This comparative study validates the success of the hybrid blade stragy in resolving the classic aero-structural trade-off inherent in wind energy engineering:

- **Aerodynamic Performance:** The power-producing outer span (r > 0.085 m) remains highly streamlined by utilizing the excellent lift-to-drag ratio of the slender SG6043 profile, ensuring optimal kinetic energy extraction and minimal skin friction.

- **Structural Integrity:** The rotor is mechanically secured at its most critical joint by using the robust SG6040 profile as a structural bridge between the circular mounting foil and the aerodynamic body. This configuration yields a wind turbine blade that maximizes aerodynamic extraction efficiency while guaranteeing long-term structural durability.

IV.9. Results

Global wind turbine technologies exhibit a wide diversity in terms of blade number, Tip Speed Ratio and blade length. Nevertheless, three-bladed Horizontal Axis Wind Turbines (HAWTs) remain the most widely deployed configuration in the wind energy sector. Within this framework, this section presents the aerodynamic performance results obtained via the computational simulation software QBlade. The rotor blade design was developed by blending two distinct aerodynamic airfoils (SG6043 and SG6040) to establish the optimal geometric and physical characteristics of the turbine rotor. To ensure simulation fidelity and achieve the targeted performance metrics, the following fundamental design and operational parameters were defined and initialized:

- **Number of Blades (NB):** Establishes the rotor solidity and dictates its direct influence on aerodynamic torque and thrust generation.
- **Tip Speed Ratio (TSR):** Defines the dimensionless ratio between the tangential velocity of the blade tip and the free-stream wind velocity.
- **Rotor Tip Radius (R_{tip}):** Determines the total rotor swept area, governing the theoretical limit of aerodynamic power extraction.
- **Hub Radius (R_{hub}):** Defines the geometric dimensions of the central structural root and delineates the aerodynamically inactive flow region.
- **Reynolds Number (Re):** Characterizes the fluid dynamic regime (laminar, transitional, or turbulent flow) to ensure precise calculation of lift and drag forces.

IV.9.1. Study of the Effect of Blade Number

To investigate the effect of varying the number of blades on the aerodynamic characteristics of the wind turbine including the absolute parameters: Power (P), Torque (M), and Thrust (T), as well as their corresponding dimensionless coefficients: Power Coefficient (Cp), Torque Coefficient (Cm), and Thrust Coefficient (Ct). The governing operational and geometric simulation parameters were held constant at the following designated values:

Free-Stream Wind Velocity (V): 6 m/s

Tip Speed Ratio (TSR): 5.5

Rotor Tip Radius (R_{tip}): 0.385m

Rotor Hub (Root) Radius (R_{hub}): 0.28m

Under these fixed structural and flow conditions, parametric simulation trials were conducted by incrementally changing the number of blades for each case, utilizing values of: 3, 6, 12, and 24 blades (NB). This systematic approach isolates the rotor solidity variable to isolate and evaluate its direct influence on inter-blade aerodynamic interference, thereby identifying the optimal blade configuration that maximizes power extraction efficiency without compromising system dynamics (figures IV.17 and IV.18).

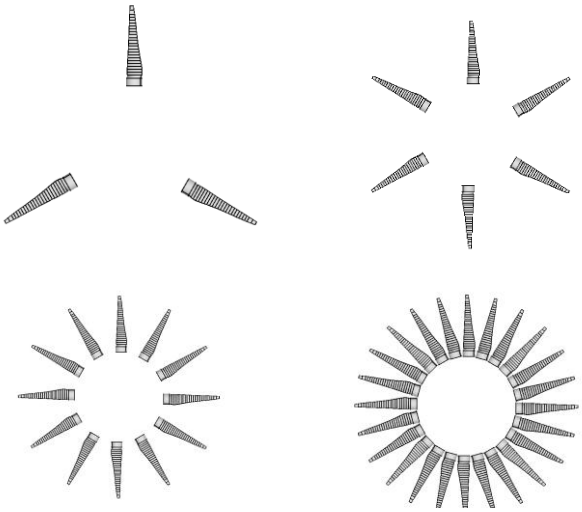


Figure IV. 17: 3D rotor geometric models with varying blade numbers (NB = 3, 6, 12, 24)

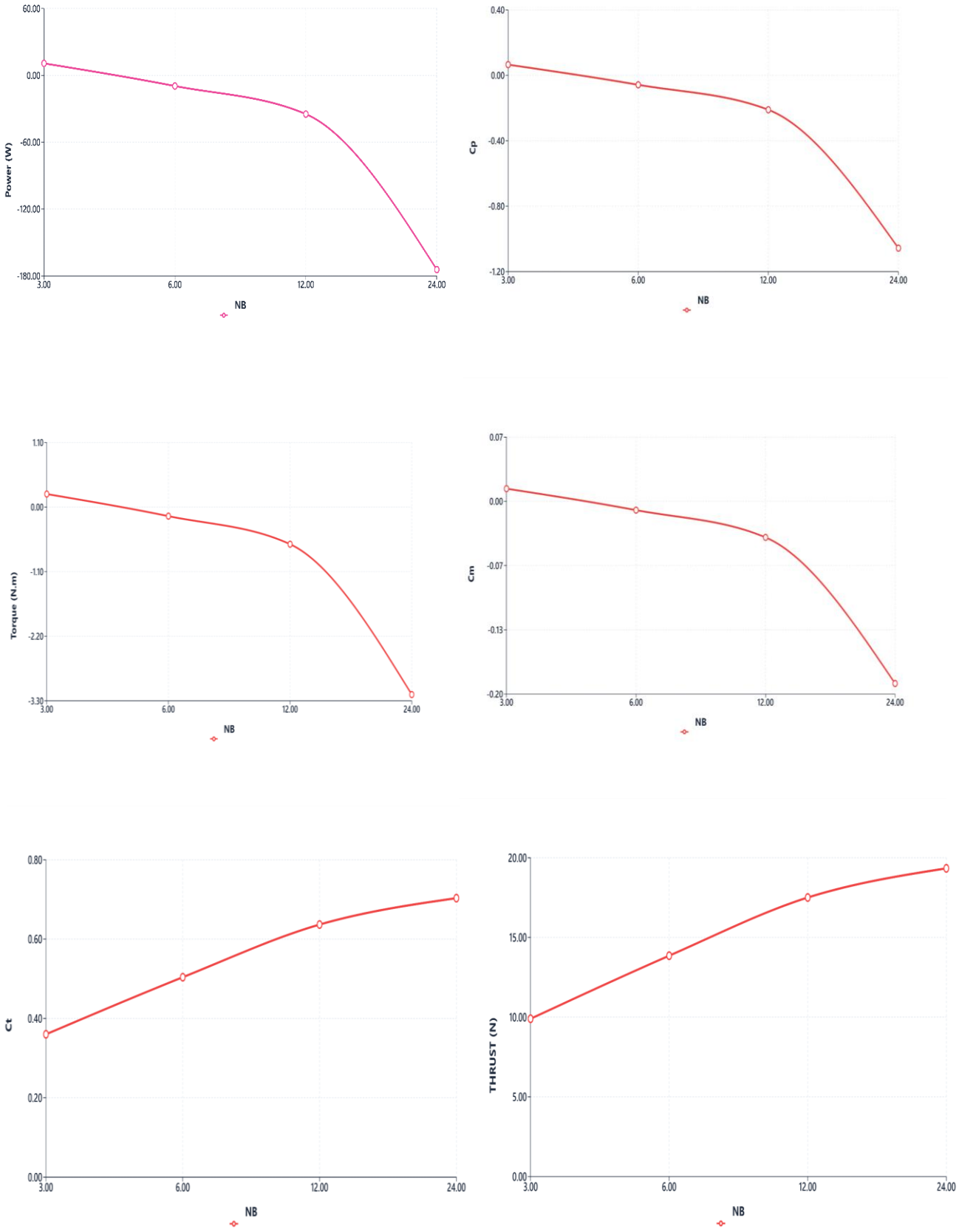


Figure IV. 18: Parametric performance curves (Power, Cp, Torque, Cm, Thrust, and Ct) as a function of blade number (NB)

Commentary and Interpretation:

substantial upgrade in the generated mechanical torque, driving a monotonic growth in net extracted power until the rotor achieves its absolute peak aerodynamic efficiency at the optimal design coordinate of N = 3. Fluid-dynamically, this positive transition is directly dictated by the scaling of rotor solidity and the expansion of the cumulative blade planform area; a higher blade count systematically amplifies the aerodynamic lift forces generated across the rotor plane by capturing a larger portion of the oncoming fluid momentum, thereby maximizing the driving aerodynamic torque at the hub interface. However, past this optimal threshold, the rate of energy extraction begins to experience a steady deceleration and eventual plateau, driven by the localized aerodynamic interference between adjacent blades and the accumulation of viscous skin friction, which counteracts the rotational driving vectors.

From a fluid-structure interaction perspective, this multi-blade upscale induces a steep, continuous expansion in the total out-of-plane axial thrust force (Thrust). This aggressive growth in thrust loading is a physical consequence of the expanded solid geometric blockage opposing the wind, which maximizes the aerodynamic pressure drop across the turbine disk. While this configuration successfully secures maximum torque and power at the design coordinate, the relentless expansion of absolute axial force imposes severe structural penalties, generating high out-of-plane bending moments that propagate down the blade span. This structural response delivers solid engineering justification for integrating the thickened hybrid root profile to absorb these intense cyclic loads, effectively redistributing peak Von-Mises stress concentrations and mitigating critical out-of-plane tip deflections.

IV.9.2. Study of the Effect of Tip Speed Ratio

To investigate the effect of varying the Tip Speed Ratio (TSR) on the aerodynamic characteristics of the wind turbine including the absolute parameters: Power (P), Torque (M), and Thrust (T), as well as their corresponding dimensionless coefficients: Power Coefficient (Cp), Torque Coefficient (Cm), and Thrust Coefficient (Ct). The governing operational and geometric simulation parameters were held constant at the following designated values:

Free-Stream Wind Velocity (V): 6 m/s

Blade Number (NB): 3

Rotor Tip Radius (R_{tip}): 0.385m

Rotor Hub (Root) Radius (R_{hub}): 0.035m

Under these fixed structural and flow conditions, parametric simulation trials were systematically executed by incrementally varying the Tip Speed Ratio (TSR) within a range from 1 to 12. This approach serves to analyze the turbine's rotational behavior relative to incoming wind velocity, thereby identifying the optimal aerodynamic operating point for maximizing energy conversion efficiency (figures IV.19).

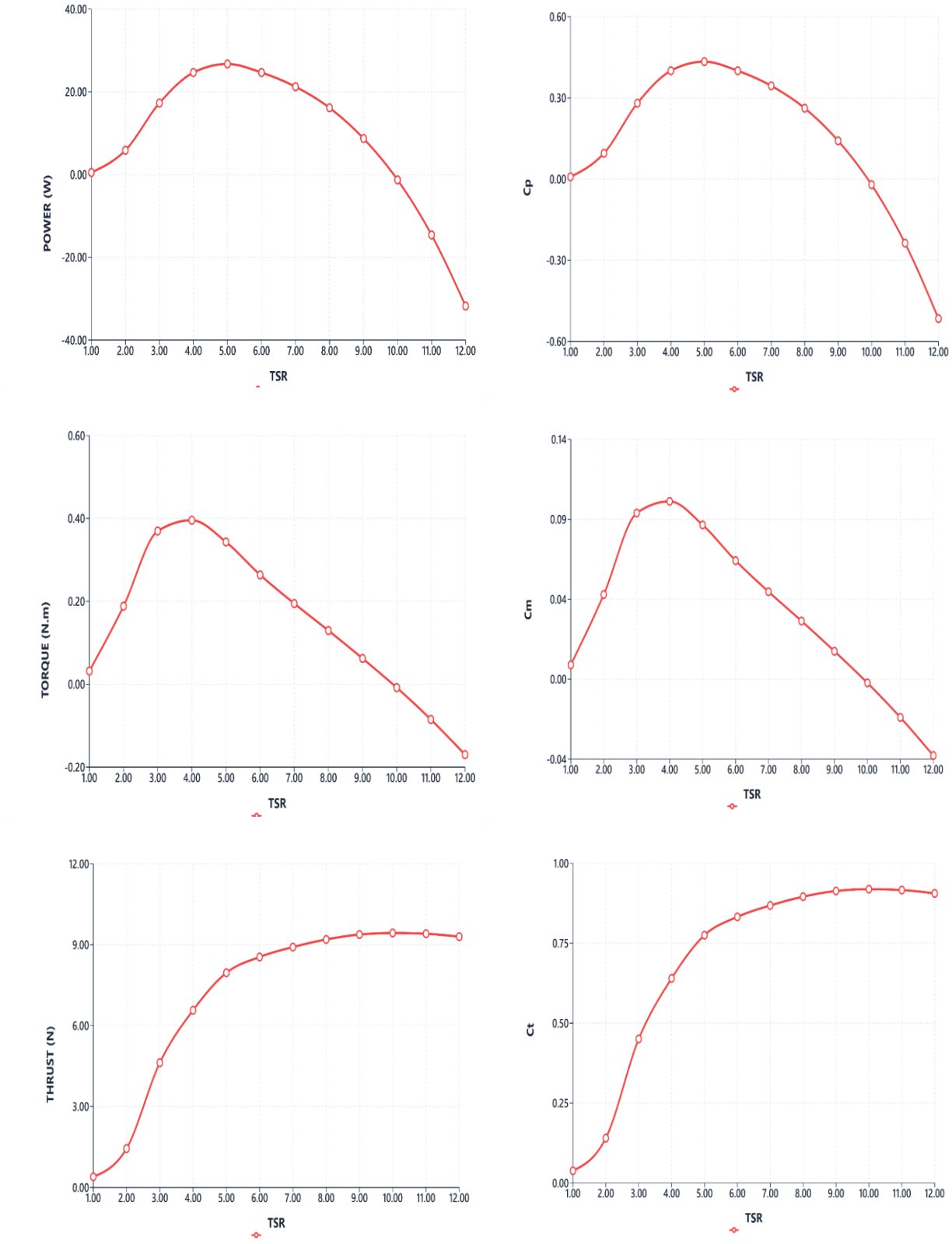


Figure IV. 19: Parametric performance curves (Power, Cp, Torque, Cm, Thrust, and Ct) as a function of TSR

Commentary and Interpretation:

The parametric evaluation spanning the tip-speed ratio spectrum reveals a standard aerodynamic response governed by three distinct physical regimes that directly dictate blade element performance. Within the aerodynamic stall regime (at low TSR), energy extraction remains highly restricted, yielding an efficiency drop near zero due to the low rotational velocity relative to the free-stream velocity, which induces massive angles of attack exceeding the design stall limit and triggers full boundary layer separation. As the rotor accelerates into the optimal design point, it achieves its absolute peak aerodynamic performance at the design sweet spot of TSR = 5.5, reaching its maximum power coefficient and net mechanical power because the relative velocity vector aligns flawlessly with the hybrid geometry to maximize the lift-to-drag ratio. Conversely, elevating the rotational speed into the high-speed choking regime triggers a severe performance collapse that pushes the turbine into negative efficiency boundaries since the hyper-rotating blades act as a solid physical disc obstructing the flow, forcing local angles of attack to near-zero or negative values and shifting lift vectors into resistive drag forces that accumulate a counter-productive braking torque. Structurally, the out-of-plane axial thrust force exhibits a steep, monotonic expansion with scaling TSR until it saturates into a critical plateau across the hyper-speed spectrum. This high-speed thrust saturation confirms maximum aerodynamic blockage, generating heavy bending moments across the blade span and fully justifying the integration of the thickened hybrid anchor geometry (SG6040) at the blade root to absorb these continuous out-of-plane forces, effectively controlling peak Von-Mises stresses and limiting catastrophic tip deflections.

IV.9.3. Study of the Effect of Blade Tip Radius

To investigate the effect of varying the rotor radius on the aerodynamic characteristics of the wind turbine including the absolute parameters: Power (P), Torque (M) and Thrust (T), as well as their corresponding dimensionless coefficients: Power Coefficient (Cp), Torque Coefficient (Cm), and Thrust Coefficient (Ct). The governing operational and geometric simulation parameters were held constant at the following designated values:

Free-Stream Wind Velocity (V): 6 m/s

Blade Number (NB): 3

Tip Speed Ratio (TSR): 5.5

Rotor Hub (Root) Radius (R_{hub}): 0.035m

Under these fixed operational conditions, parametric simulation trials were systematically performed by incrementally scaling the rotor tip radius to evaluate its direct influence, utilizing values of: 0.385 m, 0.77 m, 1.54 m and 3.08 m. This parametric study aims to analyze the aerodynamic impact of expanding the rotor swept area on both absolute mechanical loads and dimensionless conversion efficiencies (figures IV.20).

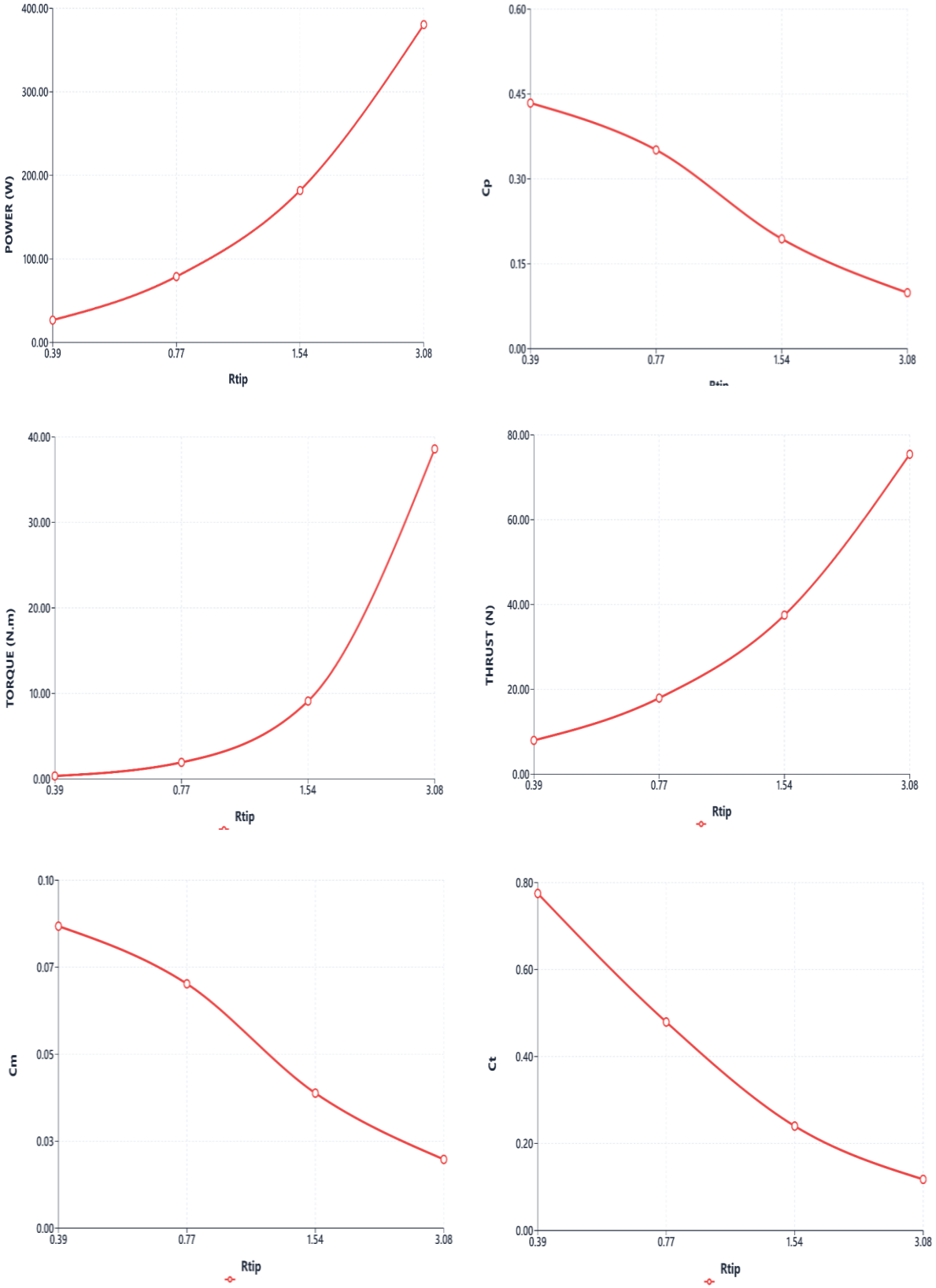


Figure IV. 20: Parametric performance curves (Power, Cp, Torque, Cm, Thrust, and Ct) as a function of R_{tip}

Commentary and Interpretation:

The numerical simulation results demonstrate that extending the blade tip radius (R_{tip}) leads to a systematic and substantial improvement across all aerodynamic performance metrics. Both the power coefficient (Cp) and the net extracted mechanical power exhibit a clear upward scaling trend, which directly correlates with a parallel expansion in the torque coefficient (Cm) and net generated aerodynamic torque. Fluid-dynamically, this continuous performance growth is governed by the expansion of the rotor swept area, which scales proportionally with the square of the radius. This geometric expansion allows the rotor to capture a significantly larger mass flow rate of air and extract a higher volume of available kinetic energy, while simultaneously increasing the moment arm length to yield higher mechanical torque at the hub interface.

From a fluid-structure perspective, this geometric upscale causes a sharp, monotonic increase in the total out-of-plane axial thrust force (Thrust), driven by the larger total surface area resisting the incoming flow. Conversely, the dimensionless thrust coefficient (Ct) follows a noticeably different trajectory, stabilizing initially before exhibiting a steady decline at larger tip radius. This localized decay in the parametric coefficient (Ct) serves as an aerodynamic indicator of shifting spanwise pressure distributions and heightened tip vortex losses as the blade aspect ratio increases. Although the declining thrust coefficient implies a relative reduction in normalized aerodynamic loading per unit area, the continuous growth in absolute axial force imposes severe bending moments along the blade span. This structural penalty reinforces the necessity of integrating the thickened hybrid root profile (SG6040) to effectively redistribute high stress concentrations and mitigate critical out-of-plane tip deflections.

IV.9.4. Study of the Effect of Rotor Hub Radius

To investigate the effect of varying the rotor hub radius on the aerodynamic characteristics of the wind turbine including the absolute parameters: Power (P), Torque (M), and Axial Thrust Force (T), as well as their corresponding dimensionless coefficients: Power Coefficient (C_p), Torque Coefficient (C_m), and Axial Thrust Coefficient (C_t). The governing operational and geometric simulation parameters were held constant at the following designated values:

Free-Stream Wind Velocity (V): 6 m/s

Blade Number (NB): 3

Tip Speed Ratio (TSR): 5.5

Rotor Tip Radius (R_{tip}): 0.385m

Under these fixed structural and flow conditions, parametric simulation trials were systematically conducted by incrementally varying the rotor hub radius, recording the performance metrics for the following distinct values: 0.035 m, 0.07 m, 0.14 m and 0.28 m. This systematic approach aims to isolate and evaluate the aerodynamic impact of expanding the central structural root on both absolute mechanical loads and dimensionless conversion efficiencies (figure IV.21).

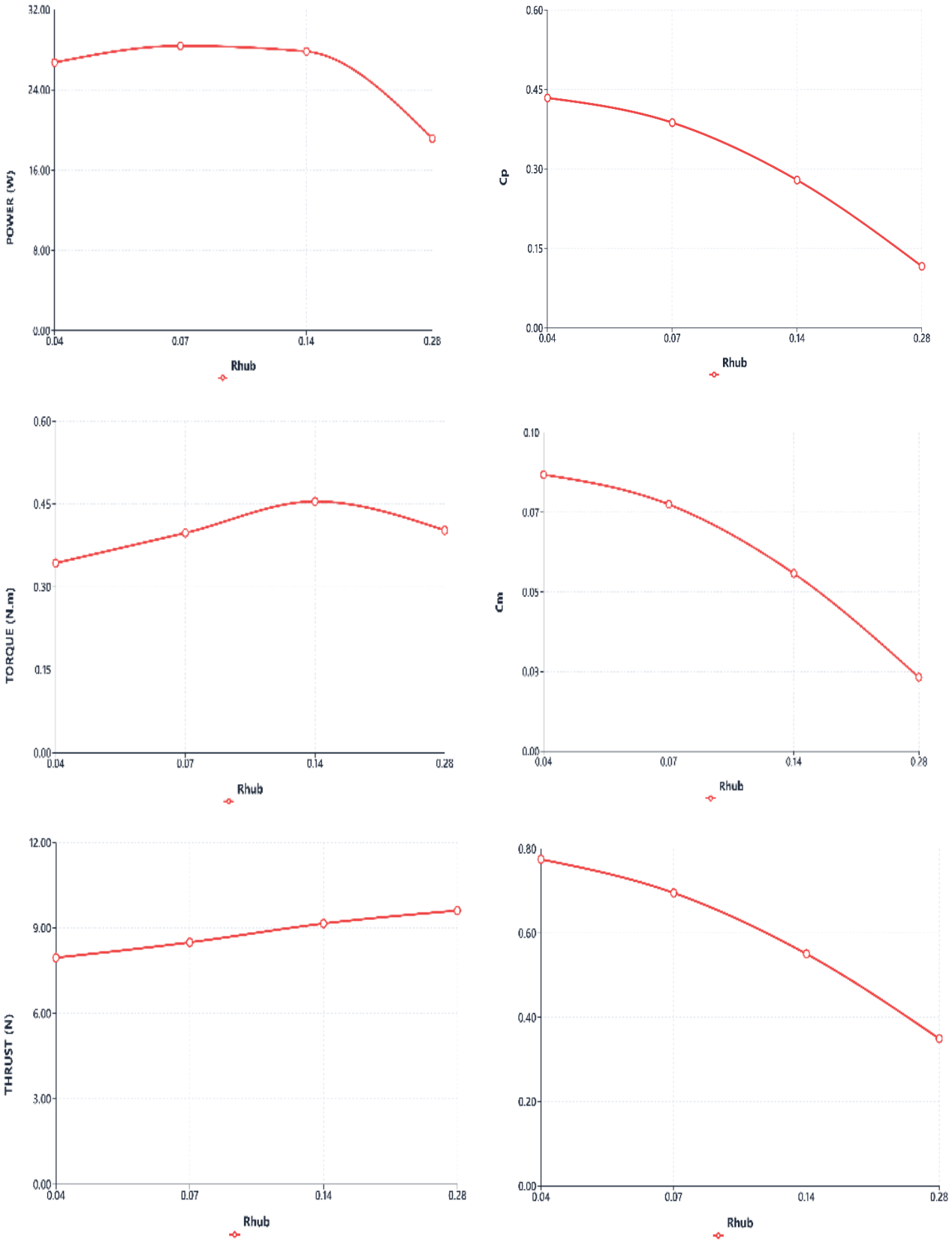


Figure IV. 21*:* Parametric performance curves (Power, Cp, Torque, Cm, Thrust, and Ct) as a function of R_{hun}

Commentary and Interpretation:

Aerodynamically, the hub represents the energetically inactive core of the total rotor swept area. Inspecting the power coefficient (Cp) and torque coefficient (Cm) profiles reveals a continuous declining trend, peaking at the minimum investigated hub radius (Rhub = 0.04 m) with a Cp of roughly 0.43 and a Cm of approximately 0.082. As the hub radius expands incrementally to 0.07 m, 0.14 m, and ultimately 0.28 m, the power coefficient undergoes a severe drop down to 0.11, while Cm collapses below 0.03. This physical degradation occurs because an oversized hub obstructs and reduces the effective kinetic swept area of the blades, penalizing the mass flow rate of air interacting with the lift-generating airfoils.

Conversely, the net Power and mechanical Torque curves exhibit an interesting parabolic trend. The net power does not peak at the smallest hub but rather ascends slightly to a maximum of 28.5 W at Rhub= 0.07 m, while the torque reaches its peak of 0.45 N.m at an intermediate before Rhub= 0.14 m both parameters collapse sharply at 0.28 m. Fluid dynamically, a hyper-compact hub (0.04 m) induces localized flow constriction and central vortex stagnation around the blended blade roots. A modest expansion to 0.07 m provides an optimal geometric transition zone, enabling the root-stationed SG6040 airfoil to operate with minimized hub-vortex penalties and generate substantial lift torque.

IV.9.5. Study of the Effect of Reynolds Number

To investigate the effect of varying the Reynolds Number (Re) on the aerodynamic characteristics of the wind turbine, including the absolute parameters: Power (P), Torque (M), and Axial Thrust Force (T), as well as their corresponding dimensionless coefficients: Power Coefficient (C_p), Torque Coefficient (C_m), and Axial Thrust Coefficient (C_t). The governing operational and geometric simulation parameters were held constant at the following designated values:

Free-Stream Wind Velocity (V): 6 m/s

Blade Number (NB): 3

Tip Speed Ratio (TSR): 5.5

Rotor Tip Radius (R_{tip}): 0.385m

Rotor Hub (Root) Radius (R_{hub}): 0.035m

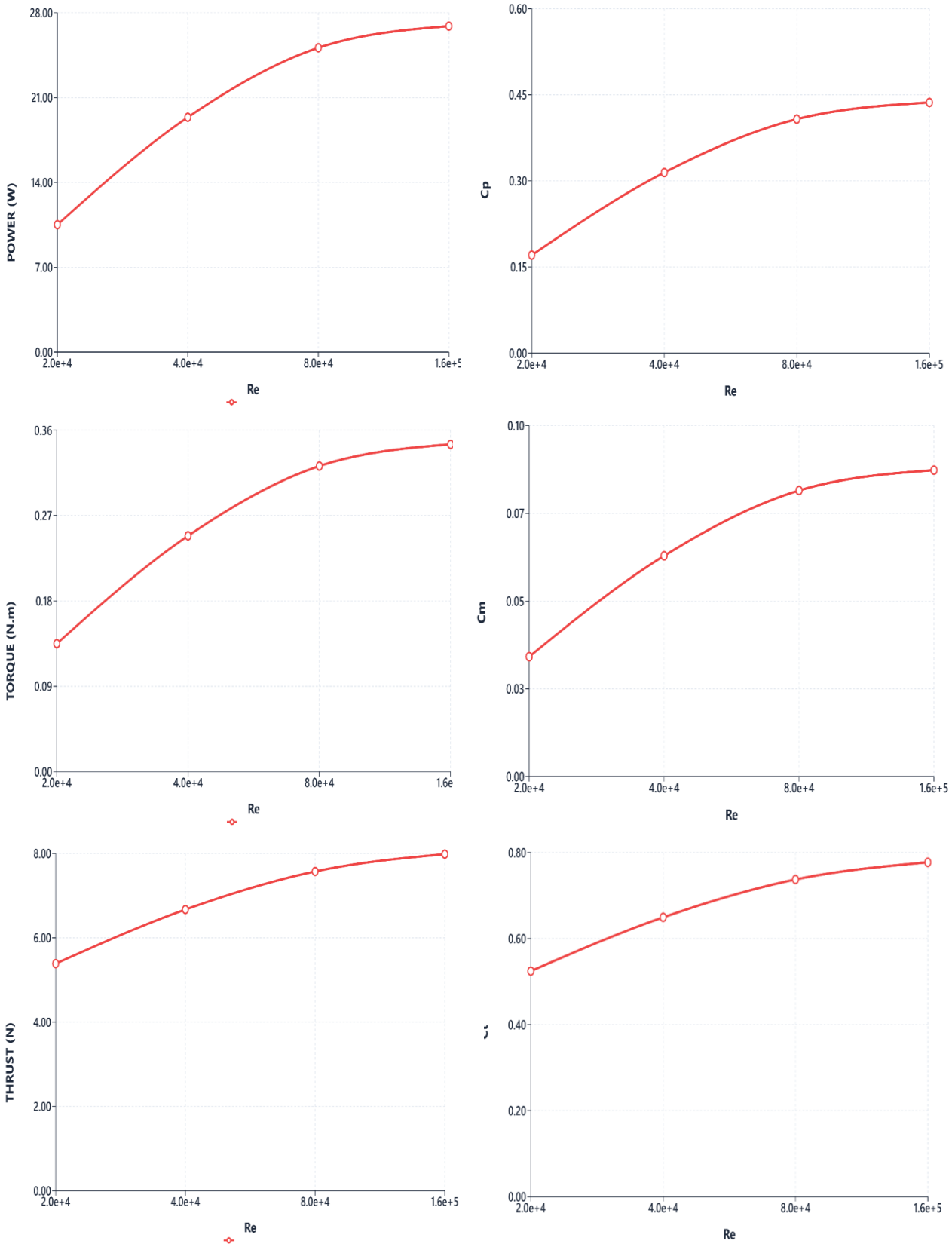


Figure IV. 22: Parametric performance curves (Power, Cp, Torque, Cm, Thrust, and Ct) as a function of R_e

General conclusion

GENERAL CONCLUSION

This research work presented a comprehensive aerodynamic design, numerical simulation, and parametric optimization of a small-scale wind turbine rotor. By systematically transitioning from fundamental wind energy concepts to advanced computational modeling, this study successfully addressed the delicate trade-off between maximizing aerodynamic efficiency and ensuring structural integrity under low Reynolds number operating conditions.

The systematic investigation conducted across the chapters yields several critical conclusions:

Aerodynamic & Structural Synergy: The implementation of a hybrid blade configuration (deploying the thicker SG6040 airfoil at the blade root and the highly efficient SG6043 airfoil at the tip) proved to be an excellent engineering strategy. This approach successfully isolated high mechanical bending moments at the root while maximizing lift generation and energy extraction at the outer span.

Theoretical Framework Validity: The Blade Element Momentum (BEM) theory, augmented with Prandtl's tip loss and Glauert's high-thrust corrections, provided a robust mathematical foundation. It allowed for rapid, high-fidelity numerical iterations within QBlade, bridging the gap between idealized actuator disk limits and real-world rotor losses.

Parametric Insights: The numerical parametric study executed in QBlade demonstrated that geometric variables such as blade count, chord distribution, twist angle, and hub radius drastically influence the power coefficient (Cp) and thrust coefficient (Ct). The optimized rotor design achieved a competitive power coefficient, aligning well with validated reference literature and proving its viability for low-to-moderate wind speed environments.

Structural Viability: The structural analysis module confirmed that the physical architecture of the blade safely sustains operational aerodynamic loads. The Von Mises stress distribution remained well within the permissible material yield thresholds, validating the structural safety of the optimized layout.

Future Perspectives

While this thesis establishes a solid foundation for the aerodynamic and structural design of small-scale wind turbines, several avenues remain open for future academic and industrial research:

Dynamic Stall & Unsteady Simulations: Extending the numerical analysis to include unsteady BEM or full Computational Fluid Dynamics (CFD) simulations to capture transient aerodynamic behaviors and dynamic stall effects in highly turbulent urban environments.

Experimental Validation: Manufacturing a physical prototype of the optimized hybrid blade using 3D printing techniques to conduct wind tunnel testing, allowing for direct validation of the QBlade numerical curves.

Aeroelastic Coupling: Performing a full aeroelastic analysis to investigate the dynamic interaction between fluid forces and blade elasticity, preventing potential catastrophic failure modes such as flutter or excessive vibrational fatigue.

Alternative Materials: Investigating the impact of advanced composite materials or eco-friendly biocomposites on reducing rotor weight while enhancing structural damping characteristics.

In conclusion, the methodologies and optimized configurations established in this thesis demonstrate that careful parametric tuning combined with advanced numerical tools can significantly push the boundaries of small-scale wind energy systems, paving the way for more reliable and efficient decentralized power solutions.

REFERENCES

[1] WIT Press, Fundamentals of Wind Energy (Vol. 44), Southampton: WIT Press, 2010.

[2] D. S. N. J. a. E. B. T. Burton, Wind Energy Handbook, 2nd ed. ed., Chichester, UK: John Wiley & Sons, 2011.

[3] J. G. M. a. A. L. R. J. F. Manwell, Wind Energy Explained: Theory, Design and Application, 2nd ed. ed., Chichester, UK: John Wiley & Sons, 2010.

[4] S. Mathew, Wind Energy: Fundamentals, Resource Analysis and Economics, Berlin: Springer, 2006.

[5] T. Wizelius, Developing Wind Power Projects: Theory and Practice, London, UK: Routledge, 2015.

[6] M. O. L. Hansen, Aerodynamics of Wind Turbines 3rd ed, London, UK: Routledge, 2015.

[7] I. Paraschivoiu, Wind Turbine Design: With Emphasis on the Darrieus Concept, Montreal, Canada: Polytechnic International Press, 2002.

[8] J. G. M. a. A. L. R. J. F. Manwell, Wind Energy Explained: Theory, Design and Application, Chichester, UK: John Wiley & Sons, 2010.

[9] Encyclopaedia Britannica, "Lift (physics)," *Britannica,* 2024.

[10] D. C. Giancoli, Physics for Scientists and Engineers with Modern Physics, Upper Saddle River, New Jersey, USA: Pearson Prentice Hall, 2008.

[11] I. H. A. a. A. E. v. Doenhoff, Theory of Wing Sections: Including a Summary of Airfoil Data, New York, USA: Dover Publications, 1959.

[12] H. S. a. J. G. Schepers, Joint Investigation of Turbine Rotor Aerodynamics, Roskilde, Denmark: Risø National Laboratory & EC (European Commission), 1995.

[13] J. B. Dragt, Wind Energy Conversion, Paris, France: Europhysics, 1993.

[14] G. P. a. J. W. David Marten, "QBlade: An Open Source Tool for Design and Simulation of Wind Turbines," *International Journal of Emerging Technology and Advanced Engineering,* vol. Vol. 3, no. No. 3, p. 635–641, 2013.